# Chapter 8
# Peculiarities of Physical Properties of Semimagnetic Semiconductors and Their Practical Application

**E.I. Gheorghitza, V.I. Ivanov-Omskii and I.T. Postolaki**

**Abstract** This chapter presents a review on studies of fundamental properties of narrow-bandgap solid solutions $Hg_{1-x}Mn_xTe$ and $Hg_{1-x-y}Cd_xMn_yTe$. The structure and parameters of energy bands, electrical, photoelectrical and photoluminescence properties of bulk monocrystals and epitaxial layers are also reviewed. The impact of manganese on the restructuring of energy spectrum of free carriers and localized states are discussed. The basic properties of semimagnetic materials $Hg_{1-x}Mn_xTe$ and $Hg_{1-x-y}Cd_xMn_yTe$ are compared with the properties of more intensively studied $Hg_{1-x}Cd_xTe$ solid solutions. It is shown that semimagnetic solid solutions $Hg_{1-x-y}Cd_xMn_yTe$ and $Hg_{1-x}Mn_xTe$ are prospective alternatives to $Hg_{1-x}Cd_xTe$ materials for the creation of infrared detector structures.

## 8.1 Introduction

Mercury telluride and cadmium telluride form a continuous series of solid solutions over the entire range of substitution compositions, whereas in the *Hg–Mn–Te* solid solution with zinc blend structure they are formed in a limited range of compositions. Although *HgTe* crystallizes in the zinc blende structure with a lattice constant a = 6.46 Å, and manganese telluride has a hexagonal structure of the *NiAs* type with lattice constant a = 4.05 Å and c = 6.71 Å, it was stated that in the *HgTe–MnTe* system a very large number of mercury atoms (over 80 %) can be substituted by manganese atoms retaining the zinc blende structure [1]. The most thoroughly studied in the group of quaternary semimagnetic alloys are $Hg_{1-x-y}Cd_xMn_yTe$.

The first studies of such a system were conducted by Delwes and Lewis [1]. Becla have shown on the basis of X-ray studies and differential thermal analysis of the phase diagram that $\alpha$-phase with sphalerite structure exists within $0 \leq y \leq 0.35$ while other

E.I. Gheorghitza · I.T. Postolaki (✉)
Tiraspol State University, Chisinau, Moldova
e-mail: postolachi@list.ru

V.I. Ivanov-Omskii
Physical-Technical Institute A. F. Ioffe RAN, 94021 St. Petersburg, Russia



I. Tiginyanu et al. (eds.), *Nanostructures and Thin Films for Multifunctional Applications*, NanoScience and Technology,
DOI 10.1007/978-3-319-30198-3_8

phases are formed in $Hg_{1-x-y}Cd_xMn_yTe$ with $y > 0.35$, that makes the material unsuitable for device structures [2]. The epitaxial growth of high-quality layers of $Hg_{1-x-y}Cd_xMn_yTe$ with $0 \le x \le 0.20$, $0 \le y \le 0.15$ has been reported [3, 4].

Peculiarities of the crystal structure and the energy spectrum of $Hg_{1-x}Mn_xTe$ as compared with non-magnetic materials have been described [5–11]. However, one significant difference between these materials and the well-known $Hg_{1-x}Cd_xTe$ was distinguished [12], namely the degree of bond ionicity and the stability of properties. The ionicity of *Hg-Te* bonds is slightly modified in ternary compounds as compared to binary compound of tellurium mercury, whereas in $Hg_{1-x}Cd_xTe$ a strong loosening of bonds takes place, leading to instability of the material properties. Therefore, $Hg_{1-x}Mn_xTe$, similarly to *HgTe*, should be much stable as compared to $Hg_{1-x}Cd_xTe$. This suggests that semimagnetic semiconductors like $Hg_{1-x}Mn_xTe$ and $Hg_{1-x-y}Cd_xMn_yTe$ are more favorable materials for the creation of infrared (IR) detectors than their non-magnetic $Hg_{1-x}Cd_xTe$ counterparts. The main parameters of $Hg_{1-x-y}Cd_xMn_yTe$, $Hg_{1-x}Mn_xTe$, and $Hg_{1-x}Cd_xTe$ solid solutions as a function of their composition have been previously reported [9, 13–15].

## 8.2 Structure and Parameters of the Energy Bands

The basic physical properties of narrow-gap semiconductor materials like $Hg_{1-x}Mn_xTe$ as well as $Hg_{1-x}Cd_xTe$ are defined by their energy structure near the point of symmetry T (center of the Brillouin zone), and in the $\vec{k} \cdot \vec{p}$ calculation of this structure it is necessary to take into consideration at least three closely spaced zones—$\Gamma_6$, $\Gamma_7$ and $\Gamma_8$. [16].

Taking into account the presence of manganese ions in the crystal lattice of $Hg_{1-x}Mn_xTe$, the so-called "modified" model of Pigeon Brown has been used for the description of the band structure of semimagnetic alloy $Hg_{1-x}Mn_xTe$ or $Hg_{1-x-y}Cd_xMn_yTe$ in a magnetic field [17–23]. This model is different from the usual one [24] by the fact that it even takes into account the exchange interaction between electrons and holes with manganese ions.

In this model the Hamiltonian is as follows:

$$\hat{H} = \hat{H}_0 + \hat{H}_{ex} = \hat{H}_0 + \vec{S}_i \sum_{\vec{R}_i} \vec{I}(\vec{r} - \vec{R}_i)\vec{\sigma}, \tag{8.1}$$

where $\vec{S}_i, \vec{\sigma}$ are spin operators of manganese ions and electrons of the conduction band; $\vec{I}$ is a constant of the electron-ion exchange splitting; $\vec{r}, \vec{R}_i$ are coordinates of the electrons and manganese ions. Since the manganese ions are located at the crystal lattice sites, and the wave function of the electron is extended, it is possible to make two simplifications.

The energy levels at the point of symmetry $\Gamma$ can be obtained by calculating the Hamiltonian in the form of a matrix (8 × 8) (D). When the asymmetrical inversion zone $\Gamma_8$ is insignificant the Hamiltonian becomes two separate matrixes (4 × 4) $D_a$ and $D_b$:

$$D = \left| \begin{matrix} \overline{D_a} & 0 \\ 0 & \overline{D_b} \end{matrix} \right| \begin{matrix} \overline{D_a} = D_a + M_a \\ \overline{D_b} = D_b + M_b \end{matrix}, \tag{8.2}$$

where $a$ and $b$ correspond to the two orientations of the electron spin:

$\vec{a}(\uparrow), \vec{b}(\downarrow)$, $D_a, D_b$ are Hamiltonian Matrix of the not modified model of Pigeon Brown, $M_a$, $M_b$ are matrix of the exchange interaction.

The contribution of the exchange interaction is taken into account by adding additional members representing the exchange integrals of electrons interaction and holes with $Mn^{+2}$ ions to the matrix of Pigeon Brown. According to calculations, the eigenvalues describing the lower levels of spin zones reducibility ($\Gamma_6$), and the upper levels of heavy holes of the valence band ($\Gamma_8$) at the point of symmetry $\Gamma$ in the parabolic approximation, have the form:

$$E_a(0) = \frac{1}{2}\hbar\omega_c + \frac{1}{2}g^*\mu_B H + 3A, \tag{8.3}$$

$$E_b(0) = \frac{1}{2}\hbar\omega_c - \frac{1}{2}g^*\mu_B H - 3A, \tag{8.4}$$

$$E_a(-1) = \hbar\omega_0\left[\frac{(\tilde{\gamma} - \gamma_1)}{2} + \frac{k}{2}\right] - B, \tag{8.5}$$

$$E_b(-1) = \hbar\omega_0\left[-\frac{(\tilde{\gamma} + \gamma_1)}{2} + \frac{3k}{2}\right] - 3B, \tag{8.6}$$

where $a(\uparrow), b(\downarrow)$ indicate the direction of the spin relative to the magnetic field;

$\omega_c$ is the cyclotron frequency of an electron in a semiconductor;
$\omega_o$ is the free electron cyclotron frequency;
$\tilde{\gamma}, \gamma_1, k$ are the modified parameters Latinzhera;
$\mu_B$ is the Bohr magneton;
$g^*$—g is the factor of an electron without the exchange interaction;
$A$ and $B$ are the contributions of the exchange interaction to the spin splitting;

$$\begin{aligned} A &= \frac{1}{6}N_0\alpha x\langle S_z\rangle \\ B &= \frac{1}{6}N_0\beta x\langle S_z\rangle \\ \langle S_z\rangle &= -S_0 B_{5/2}\left[\frac{\frac{5}{2}g_{Mn}\mu_B H}{k_B(T + T_o)}\right] \end{aligned} \tag{8.7}$$

$S_0$ is the effective spin of magnetic moment; $B_{5/2}$ is the Brillouin function; $k_B$ is the Boltzmann constant; $T_0$ is the effective temperature. $S_0$ and $T_0$ are tabulated depending on composition and temperature of the crystal.

From the (8.3)–(8.6) it is clear that the account of the exchange interaction significantly affects the spin splitting of the electron and hole states in a magnetic field. Since $g^* < 0$, and $A > 0$, the contributions from interband exchange interaction in the spin splitting are opposite, so the relative positioning of the energy sublevels $E_a(n)$ and $E_b(n)$ depend on the values of the last two terms in the (8.3)–(8.6). For samples of $Hg_{1-x}Mn_xTe$ with $x > 0.12$ there is an inequality:

$$3A > \left|\frac{1}{2}\mu_B g^* H\right| \tag{8.8}$$

It means the splitting of sublevels with different spin projections on H due to the exchange interaction is so great that the levels of the series $a(n)$ and $b(n)$ are reversed, unlike conventional narrow-gap semiconductors where $E_b(n) > E_a(n)$.

The valence band in semimagnetic semiconductors is fourfold degenerated at symmetry point $\Gamma$. As a result of the exchange interaction of holes with manganese ions, the levels of $E_a(-1)$ and $E_b(-1)$ move the energy up, unlike the non-magnetic semiconductors, where the splitting of the heavy holes is very weak.

Figure 8.1 shows the theoretical dependence of the Landau levels on the magnetic field for $H_{0.872}Mn_{0.128}Te$ when $T$ = 2 K, calculated by using the modified Pigeon Brown model [23, 25].

The dependence of the band-gap width on the composition of $Hg_{1-x}Mn_xTe$ and temperature has the form [26].

$$E_g(x,T) = (-0.253 + 3.446x + 4.9 \times 10^{-4}T - 2.55 \times 10^{-3}xT)\,\text{eV} \tag{8.9}$$

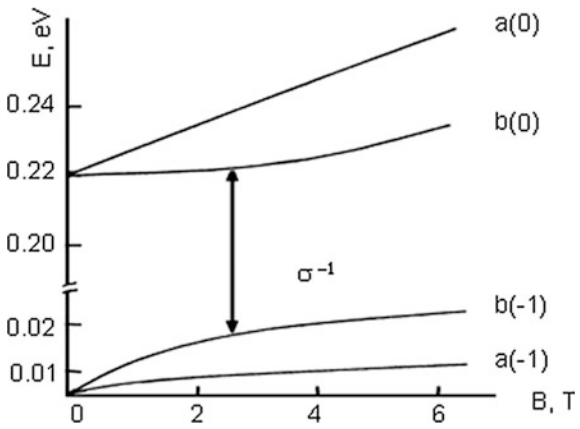


**Fig. 8.1** Theoretical dependence of the Landau levels on the induction of the magnetic field for $Hg_{1-x}Mn_xTe$ (x = 0.128) at $T$ = 2 K [23, 25]

A little different from (8.9) expression for $E_g(x,T)$ is given by Gavaleshko et al. [27] and Rogalski [9]. According to the three-band model, the effective masses of electrons and light holes in extrema are defined by:

$$\begin{aligned} m_0/m_{n0} &= 1 + (2m_0P^2/3\hbar^2)[2\varepsilon_g^{-1} + (\varepsilon_g + \Delta)^{-1}], \\ m_0/m_{l0} &= 1 - 4m_0P^2/3\hbar^2\varepsilon_g, \end{aligned} \tag{8.10}$$

where $P$ is the interband matrix element of the momentum operator, that is linearly dependent on the composition of the solid solution [28].

$$P(x) = (8.35 - 7.94x) \times 10^{-8}\,\text{eV} \cdot \text{cm}^{-3} \tag{8.11}$$

Due to non parabolic conduction band, the electron effective mass $m_n$ increases with density $n$.

$$\left(\frac{m_n}{1-m_n}\right)^2 = 32.6 \times 10^{-32}\frac{E_g^2}{p^4} + 8.32 \times 10^{-30}\frac{n^{2/3}}{p^2} \tag{8.12}$$

where $E_g$ is in eV, $p$ is in eV*cm$^{-3}$, $m_n$ is in units $m_0$.

The parameters of the valence band of $Hg_{1-x}Mn_xTe$ are not yet determined with sufficient accuracy: values of $\sim$0.5 $m_0$ [9, 26] and 0.55 $m_0$ [29] have been reported for the effective mass of heavy holes, while values of 1 eV [13] and 1.08 eV [9] have been reported for $\Delta$.

The structure and parameters of the energy bands of $Hg_{1-x}Cd_xTe$ solid solutions have been studied in many papers (see. e.g. [14, 15, 30]. It should be noted that the width of the bandgap in $Hg_{1-x}Mn_xTe$ [1, 9] changes with the composition $x$ about twice as fast as $E_g(x)$ in $Hg_{1-x}Cd_xTe$. The reason for this quantitative difference is as follows. The $\Gamma_6$ band (the conduction band in the semiconductor $Hg_{1-x}Mn_xTe$ with $E_g > 0$) is formed from $6S^2$ and $4S^2$ states of mercury and manganese. Electronic $P$—state of the tellurium forms the valence band of $\Gamma_8$ and the spin—orbit splitting of the $\Gamma_7$ band.

Since the change of the band gap width $E_g = E(\Gamma_6) - E(\Gamma_8)$ with $MnTe$ content in solid solution is related to the displacement of the $S$—zone $\Gamma_6$, a stronger dependence of $E_g(x)$ in $Hg_{1-x}Mn_xTe$ is related to greater energy difference between the $S$-levels of mercury and manganese atoms in comparison with the existing difference in the atomic levels of mercury and cadmium [5]. In particular, the semimetal-semiconductor transition, ($E_g$ = 0), in $Hg_{1-x}Mn_xTe$ corresponds to the compositions $x$ = 0.075 at $T$ = 4.2 K; $x$ = 0.066 at $T$ = 77 K; and $x$ = 0.04 at $T$ = 300 K. For comparison, the corresponding values of x in $Hg_{1-x}Cd_xTe$ equal to 0.156, 0.143 and 0.093 [31].

Partially filled and highly localized $3d^5$ ions' shell of $Mn^{2+}$ corresponds to the level (a narrow $d$-band) located in the valence band at about 3 eV below its top,

which has almost no effect on the structure of bands in the vicinity of $\Gamma$ point and, consequently, on the electrical properties of narrow-gap solid solutions [9].

However, $3d$ electrons of the manganese ions fundamentally determine the properties of $Hg_{1-x}Mn_xTe$ solid solutions. The presence of manganese ions, as described above, leads to the exchange interaction between localized magnetic moments and itinerant electrons (spin-spin $e$-$3d^5e$ $Mn^2$), which changes the zone parameters and has interesting effects on transport phenomena and optical properties in the presence of a magnetic field.

In a number of studies [5, 10, 32], devoted to the study of the energy spectrum of solid solutions $Hg_{1-x}Mn_xTe$ it is shown that in the absence of a magnetic field the energy spectrum of free and localized carriers is the same as the corresponding spectrum for $Hg_{1-x}Cd_xTe$ at the same width of the band gap. It is known that the exchange interaction in $Hg_{1-x}Mn_xTe$ is determined by the content of manganese in the solution. In order to investigate the influence of the exchange interaction it is necessary to have materials with the same band parameters but with different contents of manganese.

These requirements are satisfied by $Hg_{1-x-y}Cd_xMn_yTe$ solid solutions. It is in these semimagnetic words, that by changing the relative content of cadmium and manganese it is possible to obtain materials with the same band parameters but with different contents of manganese. Alloys of the quaternary system $Hg_{1-x-y}Cd_xMn_yTe$ in addition to purely scientific interest, which was described above, also have a special practical interest.

Previously carried our research [33, 34] confirms the possibility of creating by ion implantation photodiodes based on epitaxial layers of $Hg_{1-x-y}Cd_xMn_yTe$ ($y = 0.14$; $0.05 \leq x \leq 0.08$). It was found that the current in a range of temperatures (77–254 K) is determined by the thermal activation mechanisms, it being a diffusion mechanism at $T > 110$ K, and a generation-recombination mechanism at $T < 110$ K. The reverse currents do not exceed 1 nA at 1 V, and the value $R_0A$ at $T = 85$ K is $1.7 \times 10^7$ Ω·cm$^2$. It was shown that these values are record ones for diodes on $Hg_{1-x}Mn_xTe$ and $Hg_{1-x-y}Cd_xMn_yTe$ of similar composition. The specific detectivity at $T = 77$ K and the aperture backlight $2\pi^*sr$ is $5 \times 10^{11}$ cm * Hz$^{1/2}$W$^{-1}$. The given parameters are at the level corresponding to the best photodiodes on $Hg_{1-x}Cd_xTe$ of the given diapason. This suggests that the technology of the $Hg_{1-x-y}Cd_xMn_yTe$ material came to the same level with $Hg_{1-x}Cd_xTe$ and now it is possible to attain a better stability of photodiodes due to higher structural perfection of $Hg_{1-x-y}Cd_xMn_yTe$ solid solutions. This conclusion is supported by studies conducted in recent years [35].

The dependence of the main band parameters of $Hg_{1-x-y}Cd_xMn_yTe$ on the composition of ($x$, $y$) and the temperature is more complex than for $Hg_{1-x}Mn_xTe$. The following expression was obtained in the framework of the virtual crystal model for $E_g(x, y, z)$ [32]:

$$\varepsilon_g = \frac{(1-x-y)x \cdot \varepsilon_{12}(u) + xy \cdot \varepsilon_{23}(\upsilon) + (1-x-y)y \cdot \varepsilon_{13}(\omega)}{(1-x-y)x + xy + (1-x-y)y} \tag{8.13}$$

$$u = 0.5(2x+y) \quad \upsilon = 0.5(1-x+y \quad \omega = 0.5(2y+x)$$
$$\varepsilon_{12} = \varepsilon_g(Hg_{1-u}Cd_uTe)$$
$$\varepsilon_{23} = \varepsilon_g(Cd_{1-\upsilon}Mn_\upsilon Te)$$
$$\varepsilon_{13} = \varepsilon_g(Hg_{1-\omega}Mn_\omega Te)$$

Experimental studies of the energy spectrum of $Hg_{1-x-y}Cd_xMn_yTe$ confirmed the validity of the chosen model and the obtained analytical expression for $E_g(x, y, T)$ in the framework of this model [36, 37].

It follows from the above performed analysis of literature data that the spin-independent properties of narrow-gap $Hg_{1-x-y}Cd_xMn_yTe$ and $Hg_{1-x}Mn_xTe$ solid solutions are largely similar to those of $Hg_{1-x}Cd_xTe$ solid solutions.

## 8.3 Electrical Properties of $Hg_{1-x}Mn_xTe$ and $Hg_{1-x-y}Cd_xMn_yTe$ Semimagnetic Semiconductors

The electrical properties of $Hg_{1-x}Mn_xTe$ solid semimagnetic solutions as a function of composition, in a magnetic field and in the absence of the magnetic field, are discussed in a number of studies [8, 38–43]. This review will focus on more recent works performed on more qualitative materials.

The dependence of the intrinsic carrier concentration on the composition and temperature obtained using the Kane dispersion law and the effective mass of the heavy holes $m_p = 0.5m_0$ is [9]

$$n_i(x,T) = (4.65 - 1.59x + 0.00264T - 0.017xT + 34.15x^2) \times 10^{14}\varepsilon^{3/4}T^{3/2} \cdot \exp\left(-5802^{\varepsilon_y}/_T\right) \text{cm}^{-3} \tag{8.14}$$

where $\varepsilon_{\mathcal{H}}$ is expressed in electron volts. This expression is valid in the temperature range $17 \leq T \leq 350$ K and composition range $0.07 \leq x \leq 0.20$. The dependence is somewhat different from (8.11), and is also given in [13].

Various methods were used to obtain a sufficiently homogeneous composition of crystals and epitaxial layers of $Hg_{1-x}Mn_xTe$ solid solutions. Mani et al. [44] investigated the degree of uniformity of $Hg_{1-x}Mn_xTe$ crystals with $x = 0.125$ and $Hg_{1-x}Cd_xTe$ with $x = 0.21$ grown by solid-state crystallization, and have found that the composition distribution along the length of the ingot of these solid solutions is approximately the same. Highly homogeneous in composition ($\Delta x$ no more than 0.003) monocrystalline $Hg_{1-x}Mn_xTe$ ingots with dislocation density up to $3 \times 10^5$ cm$^{-2}$ without low-angle boundaries were obtained by zone melting in of a solution of tellurium melt [47]. Similar results were obtained when growing $Hg_{1-x}Mn_xTe$ crystals with x $\sim$ 0.1, by a modified zone melting method [45]. It should be

noted that the grown bulk crystals have p-type conductivity and typically a high concentration of charge carriers $10^{17}$–$10^{18}$ $cm^3$, caused by mercury vacancies, similarly to $Hg_{1-x}Cd_xTe$ solid solutions. However, $Hg_{1-x}Mn_xTe$ single crystals obtained by a modified vertical Bridgeman method at a rate of growing of 0.4 mm/h and temperature gradient 50 K/cm, were found to have the hole concentration $p = (1–4) \times 10^{16}$ $cm^{-3}$ and mobility $\mu_h$ =s (400–500) $cm^2$/(Vs) at the temperature of liquid nitrogen [46].

To reduce the concentration of holes and to produce electronically conductive material, the prolonged annealing of the grown crystals or of epitaxial layers of *p*-type conductivity in mercury vapor is used [45, 47–50]. Annealing leads to a drastic reduction in the mercury vacancy concentration, resulting in a material with a reduced concentration of holes or n-type material, with the free electron density of the order of $10^{15}$ $cm^{-3}$, and the mobility $\mu_n = (10^4–10^5)$ $cm^2$/(Vs) depending on the composition. The studies of galvanomagnetic properties confirm that, similarly to $Hg_{1-x}Cd_xTe$, the electron mobility is twice higher than the mobility of holes. Therefore, one can suggest that the *p*-type $Hg_{1-x}Mn_xTe$ crystals have mixed-type conductivity in a fairly wide range of temperatures. The investigations of crystals of quaternary $Hg_{1-x-y}Cd_xMn_yTe$ solid solutions by electron paramagnetic resonance method have shown that annealing in mercury vapor also leads to some redistribution of atoms and to a more ordered state [51].

Anomalies in the temperature dependence of the Hall coefficient in *p*-type $Hg_{1-x-y}Cd_xMn_yTe$ quaternary solid solutions, similar to those observed in $Hg_{1-x}Cd_xTe$, were studied by Gheorghita et al. [42]. A hopping conductivity mechanism related to the restructuring of the acceptor states due to ion exchange interaction was observed in the p-type $Hg_{1-x}Cd_xTe$ material [52–54]. These authors also explained the formation of the S-shaped current-voltage characteristic in the given material, and the occurrence of non-equilibrium distribution of charge carriers in the impurity zone at the impact ionization [53].

In contrast to $Hg_{1-x}Cd_xTe$ solid solutions, for which the behavior of impurities was studied in a large number of works (see. [55–57]), this issue is still in the early stages of research in the semimagnetic semiconductors, particularly in $Hg_{1-x}Mn_xTe$ and $Hg_{1-x-y}Cd_xMn_yTe$.

The production of high-quality epitaxial layers of $Hg_{1-x}Mn_xTe$ and $Hg_{1-x-y}Cd_xMn_yTe$ from tellurium solution-melts on substrates of cadmium telluride was reported for the first time by Bazhenov et al. [38] and Mironov et al. [58].

The electrical properties and the mechanisms of scattering of electrons and holes have been researched recently in details in a wide range from room temperature to the temperature of liquid helium in epitaxial layers of $Hg_{1-x}Mn_xTe$ with *n*- and *p*-type conductivity and with different composition [59–63]. In these studies, single-crystal layers were grown by liquid-phase method on substrates of cadmium telluride, sapphire or polished quartz from tellurium solution melts. The samples were of *p*-type conductivity with the concentration and mobility of holes about $10^{17}$ $cm^{-3}$ and 77 K. The concentration of holes was reduced and layers of n-type

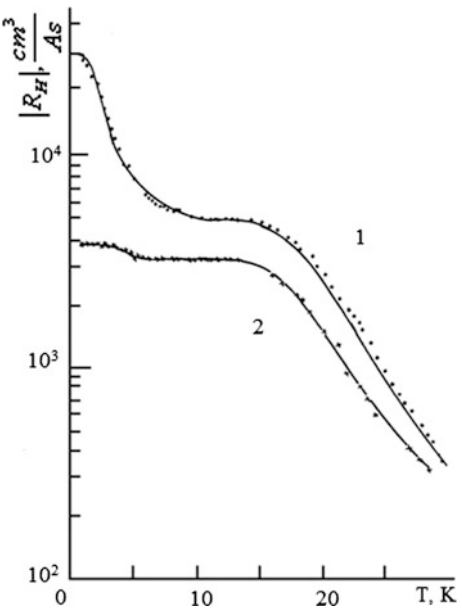


**Fig. 8.2** Dependence of Hall coefficient $R_H$ on temperature for $Hg_{1-x}Mn_xTe$; *1*—$x = 0.105$; *2*—$x = 0.095$

conductivity were obtained by annealing of samples in mercury vapor. In most of the layers of n-type conductivity, the Hall coefficient is practically constant in the region of impurity conductivity up to 4.2 K. However, in some cases there was an increase in value of $|R_H|$ at low temperatures, indicating the presence of local levels in the bandgap.

The dependence of $R_H(T)$ for two layers with $x = 0.105$ and $x = 0.095(\varepsilon_g > 0)$ is shown in Fig. 8.2.

These relationships have been explained by the presence of an energy level at about 5 meV below the conduction band along with very shallow donors and acceptors, the deep acceptor concentration being equal to $1 \times 10^{15}\,\mathrm{cm}^{-3}$ and $2.4 \times 10^{14}\,\mathrm{cm}^{-3}$ in the layers 1 and 2, respectively. The curves in Fig. 8.2 represent the solution of the equation of electrical neutrality for these two samples.

A model with two independent acceptor levels in the bandgap was adopted in order to explain the dependence $R(T)$ in the region of impurity conduction. The dashed curves in Fig. 8.3 provide solutions to the equation of electrical neutrality for these layers for the model with the following parameters:

$$\varepsilon_{a1} = 1.6\,\mathrm{meV}, \qquad N_{a1} = 6 \times 10^{15}\,\mathrm{cm}^{-3} \qquad (x = 0.08)$$
$$N_{a2} = 3 \times 10^{15}\,\mathrm{meV}, \quad N_d = 5.8 \times 10^{15}\,\mathrm{cm}^{-3} \qquad \varepsilon_{a2} = 21\,\mathrm{meV}$$

Figure 8.3 shows the temperature dependence of the Hall coefficient and electrical conductivity for two $p - Hg_{1-x}Mn_xTe$ layers with $x = 0.08$ and $x = 0.127$, (curves 1, 1′ and 2, 2′, respectively).

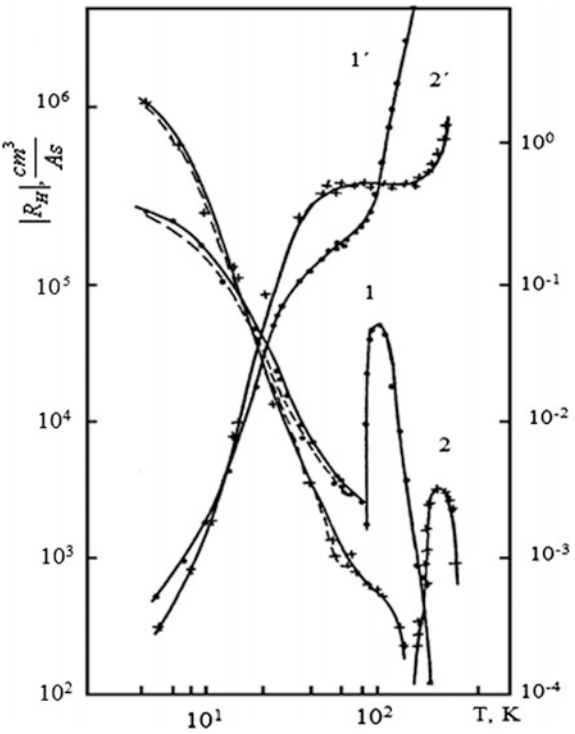


**Fig. 8.3** Dependence of $R_H$ and electrical conductivity ($\sigma$) on temperature for epitaxial layers of $p$-$Hg_{1-x}Mn_xTe$ *1*, *1′*—$x = 0.08$; *2*, *2′*—$x = 0.127$

$$\varepsilon_{a1} = 2\,\text{meV}, \qquad N_{a1} = 1.4 \times 10^{15}\,\text{cm}^{-3} \qquad (x = 0.127)$$
$$N_{a2} = 1.2 \times 10^{16}\,\text{meV}, \quad N_d = 1.38 \times 10^{15}\,\text{cm}^{-3} \qquad \varepsilon_{a2} = 19\,\text{meV}$$

Here $\varepsilon_a$ is the value of the acceptor levels energy above the valence band, $N_a$, $N_d$ are concentrations of acceptor and donor centers.

The temperature dependence on the mobility of electrons and holes in the researched layers of $n$- and $p$-type conductivity for these compositions are shown in Figs. 8.4 and 8.5.

The analysis showed that at high temperatures the main mechanism of scattering is the scattering by polar optical phonons (similarly to $Hg_{1-x}Cd_xTe$ solid solutions). In addition, Trifonova et al. suggested that one must take into account the scattering of electrons on heavy holes [60], the concentration of which is high enough and which can be regarded as fixed ions with respect to the electrons due to the large differences in their effective masses.

At low temperatures, both the electrons and holes are scattered on charged donor and acceptor centers with a total concentration in the studied layers of about (0.5–2.0) $\times$ $10^{16}$ $\text{cm}^{-3}$. The solid curves in Fig. 8.4, and the dashed curves in Fig. 8.5 present the results of theoretical calculations of $\mu_n$ and $\mu_p$, which explain satisfactorily the observed temperature dependence.

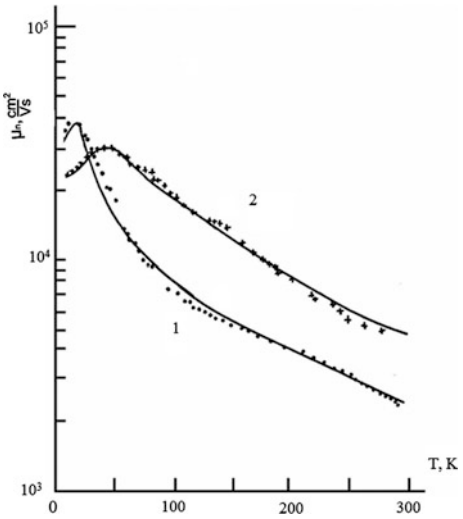


**Fig. 8.4** The temperature dependence of the electron mobility for epitaxial layers *n-*$Hg_{1-x}Mn_xTe$; *1*—x = 0.08; *2*—x = 0.127

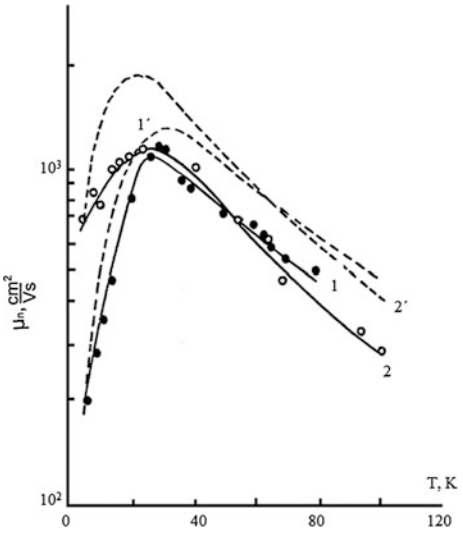


**Fig. 8.5** The temperature dependence of the mobility of holes in semimagnetic semiconductors in *p-* $Hg_{1-x}Mn_xTe$ (experiment and theory) *1,1′*—$x = 0.08$*; 2,2′*—$x = 0.127$

Extra channels of scattering due to the presence of manganese in the lattice of $Hg_{1-x}Mn_xTe$ solid solution were not revealed in the above mentioned works. In our opinion, this suggests that in the absence of a magnetic field the energy structure of semimagnetic $Hg_{1-x}Mn_xTe$ and nonmagnetic $Hg_{1-x}Cd_xTe$ alloys is, in fact, the same.

We studied in details the electrical properties of $Hg_{1-x-y}Cd_xMn_yTe$ epitaxial layers and the mechanism of electrons and holes scattering in a wide range of temperatures and compositions [38, 41, 42].

Brandt et al. reported the results of investigation of electrical properties of $p - Hg_{1-x-y}Cd_xMn_yTe$ epitaxial layers with the width of the bandgap of 250–350 meV obtained by liquid-phase epitaxy from solutions-melts enriched with tellurium [38]. Measurements of the Hall coefficient and conductivity were carried out according to standard procedures on direct current in magnetic fields 0.6–1.5 kOe in the range of temperatures of 4.2–300 K. A number of features of the temperature dependence on the Hall coefficient was identified [38]. The Hall coefficient was found to change the sign from negative to positive as the temperature decreases, this change being associated with the transition of the intrinsic conductivity to the impurity conductivity. It was also found that the Hall coefficient further increases exponentially due to the freezing of holes on a localized acceptor level.

The increase of the Hall coefficient with decreasing the temperature slows down abnormally at $T < 30$ K. This behavior of $R$ at low temperatures is typical for $Hg_{1-x}Cd_xTe$ crystals [64]. The analysis of numerous studies (see, e.g. [64]) shows that the $Hg_{1-x}Cd_xTe$ epitaxial layers obtained during the epitaxy process from solutions enriched with tellurium as well as monocrystals have p-type conductivity with concentration of uncompensated acceptors due to intrinsic defects $N_A - N_D = (0.5–5) \times 10^{17}$ cm$^{-3}$. The concentration of compensating donors $N_D$ is on the level of $10^{17}$ cm$^{-3}$. In order to reduce $N_A - N_D$ to the value of $(0.1–1) \times 10^{16}$ cm$^{-3}$, which is required for the creation of diode structures in narrow-gap semiconductors, annealing in mercury vapor is carried out. Brandt et al. suggested that the value $N_A - N_D$ in $Hg_{1-x-y}Cd_xMn_yTe$ layers is by 1–2 orders of magnitude lower as computed to epitaxial $Hg_{1-x}Cd_xTe$ layers, while the concentration of donors is at the same level [38]. It was also suggested that the proximity of values of $\varepsilon_A$ in $Hg_{1-x}Cd_xTe$ and $Hg_{1-x-y}Cd_xMn_yTe$ reflects the similar nature of the acceptors, which are associated, most probably, with intrinsic defects of a similar nature. Their lower concentration determines a narrower region of homogeneity in this system with respect to the defects acting as acceptors, which are associated with the introduction of the manganese in the composition of solid solution.

## 8.4 Photoelectrical Properties

The processes of generation and recombination of carriers basically determine the operation of the most important types of semiconductor devices such as radiation detectors, lasers, transistors, photodiodes, phototransistors, etc. The processes determine the lifetime of nonequilibrium charge carriers—a basic photoelectric parameter of semiconductor materials.

The investigation of photoelectrical properties of bulk single crystals and epitaxial layers of $Hg_{1-x}Mn_xTe$, $Hg_{1-x-y}Cd_xMn_yTe$ as well as investigation of non-equilibrium processes has been started quite recently. Let us review the results of this study carried out in a magnetic field as well as in the absence of a magnetic field.

### 8.4.1 Photoelectrical Properties of $Hg_{1-x}Mn_xTe$ and $Hg_{1-x-y}Cd_xMn_yTe$ in the Absence of Magnetic Field

A first study of photoconductivity of semimagnetic $Hg_{1-x}Mn_xTe$ alloys at low temperatures was reported by Gelmont et al. [65]. The authors measured the photoconductivity spectra of $Hg_{1-x}Mn_xTe$ single crystals with $0.13 \leq x \leq 0.15$ and $0.2 \leq x \leq 0.30$, grown by the Bridgeman method ($p \sim 10^{18}$ cm$^{-3}$) and annealed in mercury vapour ($p = 3 \times 10^{15}$–$2 \times 10^{16}$ cm$^{-3}$ at 77 K). Two peaks identified as "band-to-band" and "acceptor-to-conduction band" transitions have been found in the photoconductivity spectra of samples with any composition. The lifetime of carriers was measured to be around (6–9) μs.

The recombination of nonequilibrium charge carriers in $Hg_{1-x}Mn_xTe$, $Hg_{1-x-y}Cd_xMn_yTe$ bulk crystals was studied in a series of papers [45, 65–72]. Recombination centers with energy level around 110 meV above the valence band have been detected by means of deep level transient spectroscopy in $Hg_{1-x}Mn_xTe$ of $p$-type conductivity with $x = 0.18$ and $x = 0.20$ [69]. The concentration of these centres and their effective capture cross section of holes and electrons were found to be $5 \times 10^{15}$ cm$^{-3}$ and $10^{-17}$ cm$^{-2}$, respectively. The recombination of carriers was also analysed in single crystals grown by a modified method of zone melting and annealed in mercury vapour in order to homogenize the solid solution and to reduce the concentration of charge carriers [45, 70, 71]. It was found that the lifetime of no equilibrium charge carriers in the temperature range from room temperature to liquid nitrogen in the $p - Hg_{1-x}Mn_xTe$ material with the composition $x \sim 0.1$ with uncompensated acceptor concentration $10^{15}$–$10^{16}$ cm$^{-3}$ is determined by the impact recombination processes, namely, by the impact recombination in collisions of heavy holes with transmission of the released energy to the light holes and by the impact recombination in electron-electron collisions [70]. In contrast to this, in $n - Hg_{1-x}Mn_xTe$ obtained by $p \rightarrow n$ conversion of conductivity as a result of crystal annealing, the lifetime in the region of impurity conduction (at low temperature) was found to be determined by carrier recombination on Shockley-Reed centres with an energy level located at 65–67 meV above the top of the valence band [45]. According to estimations, the concentrations of recombination centres in the investigated crystals are in the range from $4.7 \times 10^{14}$ to $1.7 \times 10^{15}$ cm$^{-3}$.

Two recombination levels situated about 125 meV and 70 meV above the valence band top were found in wider bandgap $n - Hg_{1-x-y}Cd_xMn_yTe$ $x = 0.28$–$0.35$; $y = 0.01$–$0.02$ quaternaly compounds [71]. The position of these levels is close to the energy levels of recombination centres found in $Hg_{1-x}Mn_xTe$ crystals [45, 69]. The photoconductivity spectra of epitaxial $Hg_{1-x}Mn_xTe$ layers grown by a combined procedure using vapour-phase and liquid-phase epitaxy as well as the photoconductivity spectra of bulk single crystals consist of two bands associated with band-to-band and level-to-band transitions [73, 74]. The distance between the peaks in the photoconductivity spectra increases from 15 to 55 meV when the content of manganese telluride in layers is increased from 12 to 15 %. The lifetime changes slightly at low temperatures (77–110) K in layers with local inhomogeneity

of the electron density at the surface, and this lifetime is always longer than the one in electrically homogeneous samples.

The recombination and trapping processes of nonequilibrium charge carriers in compensated $Hg_{1-x}Mn_xTe$ layers with $x \sim 0.1$ $n,p < 10^{15}$ cm$^{-3}$ at 77 K, grown by liquid phase epitaxy and subjected to prolonged annealing in mercury vapour, have been studied in details in a series of papers [75–77]. The results of these studies demonstrated that the lifetime in the region of intrinsic conductivity is limited by the impact recombination processes, while it is determined by the recombination on Shockley-Reed centres in the extrinsic region. The energy levels of recombination centers in p-type layers are situated at (26–30) meV below the conduction band bottom, while they are located at about 50 meV above the valence band top in n-type layers [73] (Fig. 8.6).

At low temperatures ($T \leq 70$ K for the n-layers and $T \leq 25$ K for p-layers) the lifetime is determined by recombination through these levels and by trapping of minority non-equilibrium carrier on shallow levels (8–10) meV (Fig. 8.7). The recombination of carriers has been also investigated in $Hg_{1-x}Mn_xTe$ and $Hg_{1-x-y}Cd_xMn_yTe$ grown by liquid phase epitaxy [78–80]. It should be noted that there are many similarities in the photoelectric properties of $Hg_{1-x}Mn_xTe$ solid solutions with $x$ = 0.1–0.5 and the more intensively studied $Hg_{1-x}Cd_xTe$ solid solutions with $x$ = 0.2–0.3 (for comparison, see, e.g. [81–84]).

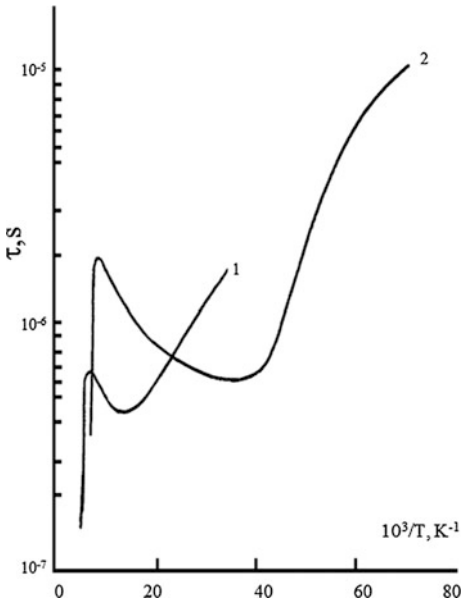


**Fig. 8.6** Dependence of the lifetime (τ) on *1/T* for $Hg_{1-x}Mn_xTe$; *1*—*n*-type; *2*—*p*-type

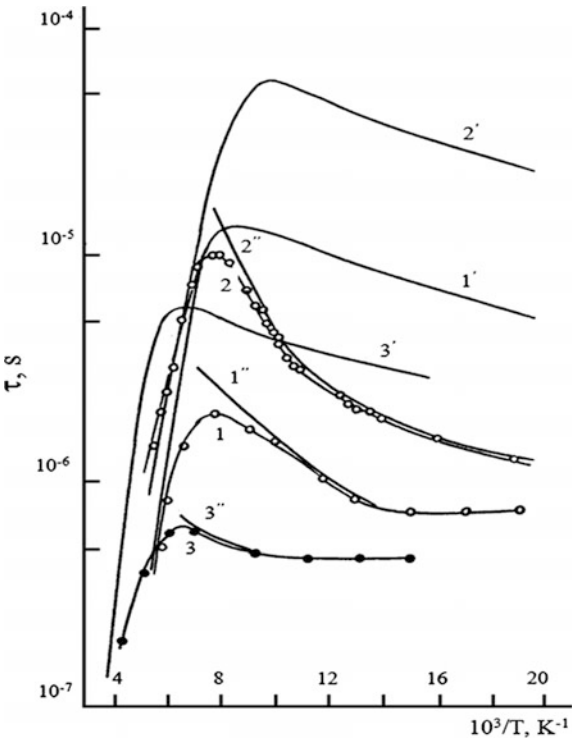


**Fig. 8.7** The temperature dependence of the lifetime of nonequilibrium charge carriers in $Hg_{1-x}Mn_xTe$ epitaxial layers. (*1*: $x = 0.097$ and $N_a - N_d = 4 \times 10^{14}$ cm$^{-3}$; *2*: $x = 0{,}10$ and $N_a - N_d = 1 \times 10^{14}$ cm$^{-3}$; *3*: $x = 0.11$ and $N_d - N_a = 5.5 \times 10^{14}$ cm$^{-3}$; *1′, 2′, 3′*—lifetimes due to the inter-band recombination processes *r, 1, 7; 1″, 2″, 3″*—lifetimes due to recombination on Shockley—Reed centers)

## 8.4.2 Photoelectrical Properties in a Magnetic Field

As shown above, in the absence of the magnetic field the properties of $Hg_{1-x}Mn_xTe$, $Hg_{1-x-y}Cd_xMn_yTe$ semimagnetic semiconductors are similar to those of conventional non-magnetic semiconductors of the $Hg_{1-x}Cd_xTe$ type, having similar band parameters. The exchange interaction caused by the presence of manganese ions in the lattice results in a substantial rearrangement of the energy spectrum of free and localized carriers when a semimagnetic semiconductor is placed in an external magnetic field. The corresponding photoelectric properties of semimagnetic semiconductors will also change significantly under the influence of the exchange interaction.

The photoconductivity spectra of $p - Hg_{1-x}Mn_xTe, (0.2 \leq x \leq 0.25)$, $(0.12 \leq x \leq 0.15)$; single crystals and $p - Hg_{1-x-y}Cd_xMn_yTe$ epitaxial layers in a magnetic field at helium temperatures have been measured in a series of papers [65–68, 72, 73, 82]. The photoconductivity was measured in the Faraday geometry $\vec{q} \left\| \vec{B} \perp \vec{E} \right.$, where $\vec{q}$ is the electromagnetic wave vector. It was experimentally found that the photoconductivity signal for $Hg_{1-x}Mn_xTe$ sharply decreases with increasing magnetic field intensity [65, 66], when the magnetic field is turned on, in

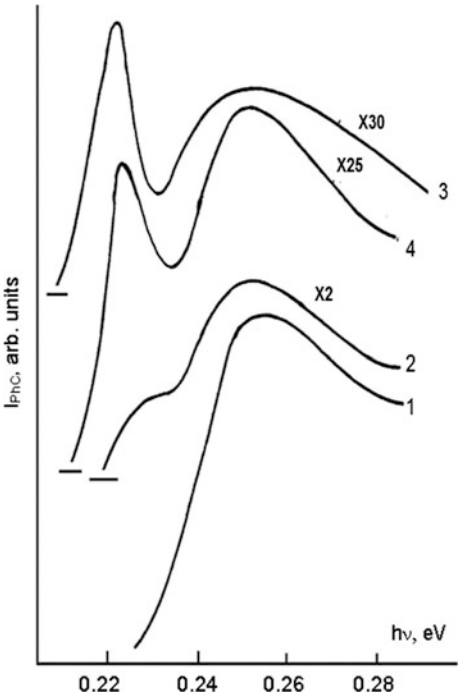


**Fig. 8.8** Photoconductivity spectra in a magnetic field for the sample $Hg_{0.86}Mn_{0.14}Te$ at $T$ = 4.2 K

contrast to $Hg_{1-x}Cd_xTe$, while the spectrum of photoconductivity shifts abnormally to longer wavelengths.

The study of photoconductivity in a magnetic field has shown that the photoconductivity signal has a non-monotonic dependence on the magnetic field strength. Figure 8.8 shows the spectra of photoconductivity for $Hg_{0.86}Mn_{0.14}Te$ measured in an external magnetic field. A long-wavelength peak appears as the magnetic field gets stronger. This peak increases in intensity and shifts to longer wavelengths with increasing the magnetic field strength.

Georgitse et al. measured the photoconductivity in a magnetic field under the excitation by circularly polarized light $\sigma^+, \sigma^-$ [66], and found that photoconductivity spectra have a complex structure. For instance, Fig. 8.9 shows the photoconductivity spectra of the $p - Hg_{0,78}Mn_{0,22}Te(\sigma^+, \sigma^-)$ alloy in a magnetic field of $B = 6T$ at 4.2 K and the photoluminescence spectrum of the same alloy in the same field. These investigations confirmed that the fine structure observed in the photoconductivity spectra measured in both $\sigma^+$ and in $\sigma^-$ polarizations can be associated with the paramagnetic band splitting. The identification of the observed structure is performed taking into account the selection rules and by comparing the experimental spectra with the results of calculations with the following parameters: the width of the bandgap and the manganese content $\varepsilon_H = 0.533\,\text{eV}; x = 0.22$; the exchange interaction integral for the conduction band $N_0\alpha = -0.45\,\text{eV}$; the effective temperature $T_0 = 54\,\text{K}$; the effective spin $S_0^{(n)} \sim 1$. The following transitions

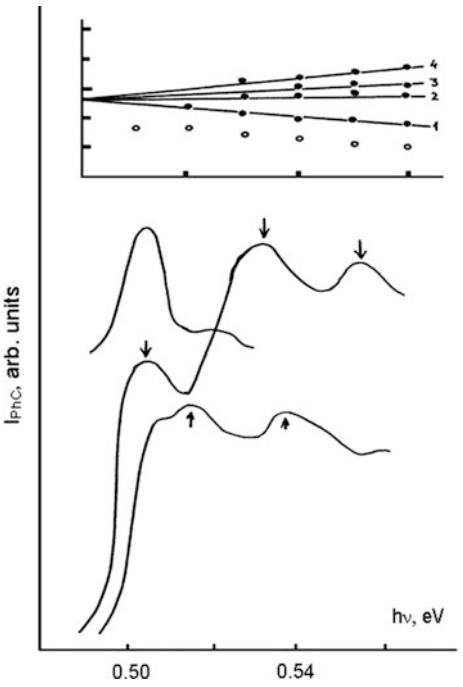


**Fig. 8.9** Photoconductivity spectra of the alloy $Hg_{1-x}Mn_xTe$ at $\sigma^+(1)$ and $\sigma^-(1)$ polarization in a magnetic field $B = 6T$

are identified in $\sigma^-$ polarization $b_n(-1) \rightarrow b_c(0); a_n(-1) \rightarrow a_c(0)$, and in $\sigma^+$ polarization $b_n(1) \rightarrow b_c(0); a_n(1) \rightarrow a_c(0)$, as well as the impurity transition in $\sigma^+$ polarization $|-3/2> \rightarrow b_c(0)|$.

As one can see from the results shown in Fig. 8.9, the authors supposed that the low-energy shoulder at the edge of photoconductivity (Peak 1) in $\sigma^-$ polarization corresponds to the transition $|+3/2> \rightarrow a_c(0)|$. The estimated paramagnetic splitting of the ground state of the acceptor, defined as the difference between the energies of $|-3/2> \rightarrow b_c(0)|$ and $|+3/2> \rightarrow a_c(0)|$ transitions proved to be around 3 meV in a field of $6T$.

Further, by using the experimentally determined value of the paramagnetic spin splitting, a value of $\sim 10$ was obtained for the g factor of a hole on the acceptor ($g^h_{eH}$). By using this estimate for $g^h_{eff}$, the value of $S_0^{(h)}$ was calculated with the following fitting parameters of the valence band: the exchange integral $N_0\beta = 0.80\,\text{eV}$, the effective mass of the heavy holes $m^*_{hh} = 0.4m_0$. The effective spin $S_0^{(h)}$ of the manganese ions $Mn^{++}$ in the acceptor proved to be of the order of $\sim 0.1$. These results are consistent with data obtained from optically detected magnetic resonance (ODMR) studies for this alloy [85].

## 8.5 Photoluminescence Properties

### 8.5.1 *Photoluminescence Properties in the Absence of Magnetic Field*

The first results concerning the research of photoluminescent properties of $Hg_{1-x}Mn_xTe$ single crystals with $(0.13 \leq x \leq 0.3)$ and $Hg_{1-x-y}Cd_xMn_yTe$ epitaxial layers have been published at the very beginning of 90th [66–68, 72]. A combined research of photoconductivity and photoluminescence in the reflection and transmission geometries allowed one to identify the observed structure of the photoluminescence spectra. Typical photoluminescence spectra in the absence of a magnetic field for $p - Hg_{1-x}Mn_xTe$ measured at 4.2 K are shown in Fig. 8.10.

The short-wavelength band *B* in the photoluminescence spectrum corresponds to the interband radiative transitions. The long-wavelength band *A* in the spectrum is related to "conduction band—acceptor" transitions according to its energy position and behaviour. The intensity of the band *A* decreases with decreasing the concentration of the acceptor. A similar structure was revealed in the photoluminescence spectra of alloys in the absence of a magnetic field.

Georgitse et al. reported the results of a photoluminescence study of $Hg_{1-x}Mn_xTe(0,19 \leq x \leq 0,30)$ solid solutions in a temperature range of 2–200 K in the absence of a magnetic field [68]. It was shown that in alloys enriched with manganese there are optical transitions between states strictly connected to the valence band. These states, along with shallow acceptors, are related to anti-bonding states with an incomplete d-shell $Mn^+(3d^6)$ in the bandgap on the shallow acceptor level, usually attributed to intrinsic defects. An energy model was proposed in this paper which explains the observed features of the photoluminescence spectra. According to this model, the level related to manganese $Mn^+$ in $Hg_{1-x}Mn_xTe(x<0,20)$ diluted semimagnetic alloys is located in the conduction band and it is not revealed in radiative processes. However, this level goes into the

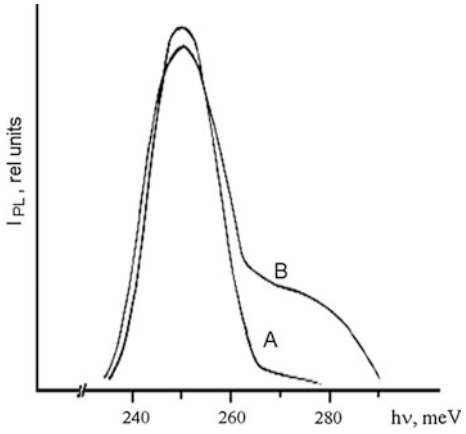


**Fig. 8.10** Photoluminescence spectrum $p$-$Hg_{1-x}Mn_xTe$ ($x$ = 0.14) at $T$ = 4.2 K

bandgap in samples with $x > 0.20$ and it participates in recombination processes. The degeneration of the $Mn^+$ level with the conduction band is lifted in samples with $x = 0.24$, while the depth of the $3d^5(Mn^{++})$ level in the valence band is estimated to be around 4.9 eV.

The analysis of $Hg_{1-x}Mn_xTe$ and $Hg_{1-x-y}Cd_xMn_yTe$ photoluminescence spectra for a wide range of temperatures in the absence of a magnetic field allowed to defined the dependence on the bandgap width upon temperature and composition of alloys [65, 67]. The depth of the acceptor level participating in radiative transitions was found to be around 18–20 meV, and it was attributed to intrinsic defects (mercury vacancies).

New papers have been published in recent years concerning the study of optical of narrow-gap semimagnetic semiconductors [86–99].

Mazur [91] investigated the photoluminescence spectra of $Hg_{0.651}Cd_{0.335}Mn_{0.014}Te$ at low temperatures (Figs. 8.11 and 8.12) by means of photoluminescence excitation spectroscopy technique described by Fuchs et al. [9, 100]. The results led to the conclusion about the observation of exciton states in narrow-gap semimagnetic semiconductors [91].

### 8.5.2 Photoluminescence Properties in a Magnetic Field

The first results concerning the research of photoluminescent properties of $Hg_{1-x}Mn_xTe$ and $Hg_{1-x-y}Cd_xMn_yTe$ alloys in a magnetic field at low temperatures have also been published at the very beginning of 90th [66–68, 72]. It was found in these works that the intensity both *A* and *B* bands increases significantly when the magnetic field is turned on at low temperatures, and their maximum shifts to the

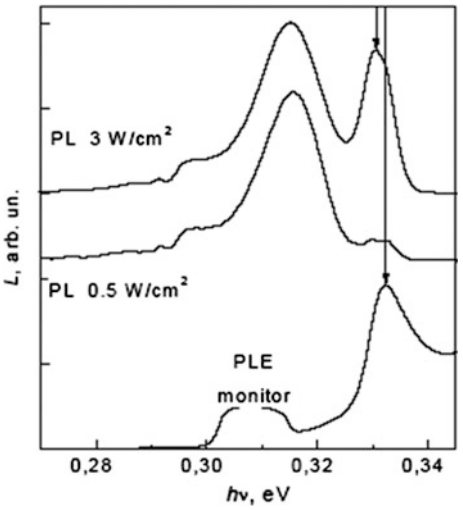


**Fig. 8.11** The photoluminescence spectra (at the *top*) $Hg_{0.651}Cd_{0.335}Mn_{0.014}Te$ measured at temperature T = 12 K, at two levels of excitation [114]

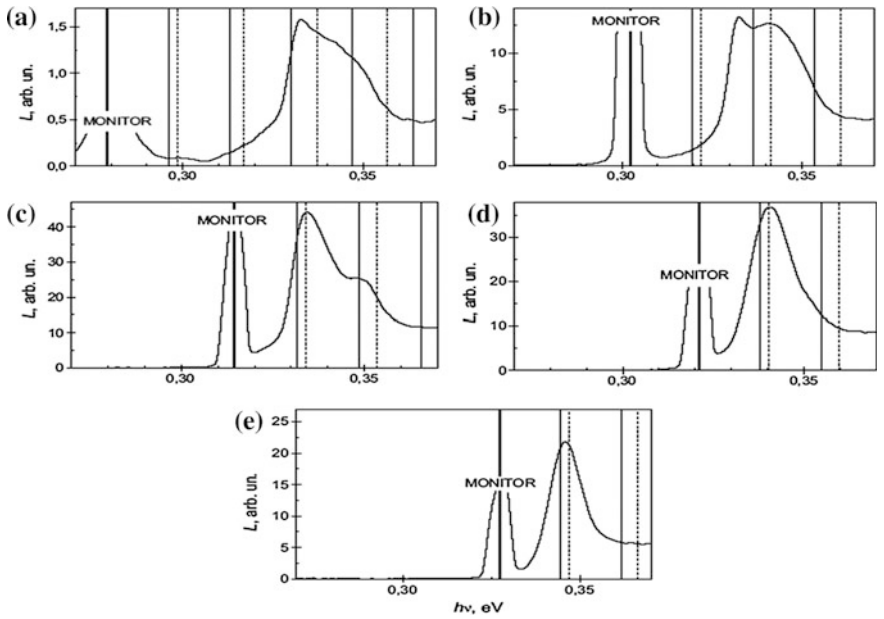


**Fig. 8.12** The Photoluminescence excitation spectra at different positions of the monitor: **a** 279.0 meV; **b** 302,5 meV; **c** 314.5 meV; **d** 321.0 meV; **e** 327.5 meV. *Direct* and *dashed vertical lines* indicate the position of the phonon replicas and monitor lines ($E_m + nE_{LO}$, where $n$ is an integer)

long wavelength region of the spectrum with increasing the magnetic field strength (Fig. 8.13), in contrast to conventional semiconductors $Hg_{1-x}Cd_xTe$, *InSb*, in which the photoluminescence bands shift to short wavelengths, and their intensity remains practically unchanged. Besides the shift of the maxima of photoluminescence bands to the long wavelengths region of the spectrum in a magnetic field, the decrease of the distance between them was also observed in the experiment. It was shown that the dependence of the radiation intensity non-monotonically varies with changing the magnetic field strength (Fig. 8.14) [67].

In weak magnetic fields the photoluminescence intensity increases rapidly with increasing magnetic field strength and it reaches a maximum at a certain value of $B = B_{\max}$. The value $B_{max}$ depends on the composition, on the content of manganese, it being shifted toward large fields with increasing the manganese content in the crystal lattice of the semimagnetic alloy. A significant increase in photoluminescence intensity was observed in a magnetic field. For instance, for the band A in a $Hg_{1-x}Mn_xTe$ ($x$ = 0.13) sample the photoluminescence intensity at $B = B_{\max}$ increases by about 50 times as compared to the photoluminescence intensity at $B$ = 0. At the same time, a further increase of the strength of the magnetic field $B > B_{\max}$ leads to a decrease in the photoluminescence intensity. In a magnetic field the radiation is polarized [89].

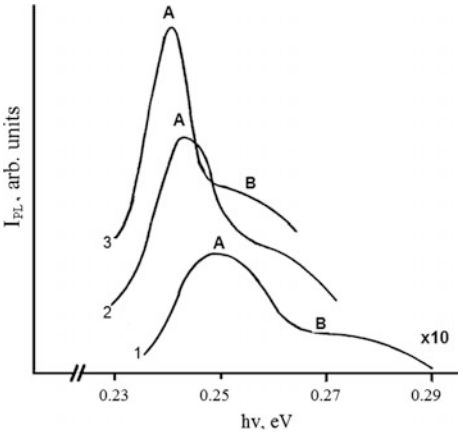


**Fig. 8.13** The photoluminescence spectra in a magnetic field of the alloy $Hg_{1-x}Mn_xTe$ ($x = 0.14$) at 4.2 K. (*1*) $B = 0$; (*2*) $B = 0.5T$; (*3*) $B = 1.0T$

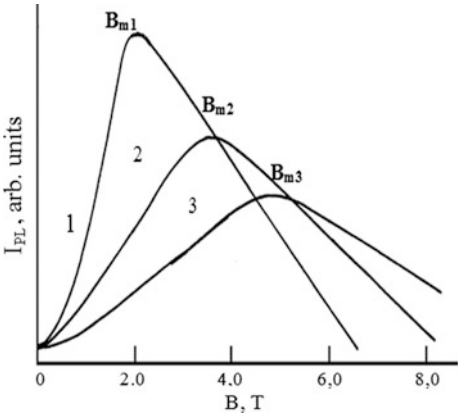


**Fig. 8.14** The experimental dependence of the photoluminescence intensity $Hg_{1-x}Mn_xTe$ on the magnetic field induction for the three compositions: *1*—$x = 0.13$; *2*—$x = 0.14$; *3*—$x = 0.15$

A similar situation was observed in $Hg_{1-x-y}Cd_xMn_yTe$ quaternary alloys [72]. The observed peculiarities of photoluminescence of $Hg_{1-x}Mn_xTe$ and $Hg_{1-x-y}Cd_xMn_yTe$ semimagnetic alloys are explained on the basis of the Pigeon Brown model taking into account the exchange interaction. The energy of other transitions allowed by the selection rules in the Faraday or Voigt geometry increases with increasing the magnetic field strength. Taking into account the population of the sublevels at low temperatures and the large value of the spin splitting, Galazka et al. suggested in their experiments that the short-wavelength band B corresponds to the interband radiative transition $b_{\Gamma_8}(0) \rightarrow b_{\Gamma_6}(-1)$, which actually determines the width of the bandgap in the magnetic field [67]. Therefore, the displacement of the *B*-band maximum in the long-wavelength region of the spectrum with increasing the magnetic field strength is a direct consequence of the restructuring of the semimagnetic semiconductor energy spectrum as a result of the exchange interaction.

It was show that, in the frame of the proposed model, the energy decreases only for the transition $b_{\Gamma_8}(-1) \rightarrow b_{\Gamma_6}(0)$ with increasing the magnetic field strength in the Faraday configuration in $\sigma^-$ polarization.

The unusual behavior of the dependence of photoluminescence intensity upon the magnetic field strength was explained taking into account the behavior of the energy acceptor energy in semimagnetic semiconductors placed in a magnetic field [101]. In was shown that the exchange interaction of holes with manganese ions leads to a sharp decrease of the acceptor ionization energy in relatively weak magnetic fields, when the exchange interaction energy is larger than the acceptor ionization energy $\varepsilon_A$ at $B = 0$, in semi-magnetic $Hg_{1-x}Mn_xTe$ alloys with fourfold degenerated valence band in the Γ-symmetry point.

Therefore, if in the absence of the magnetic field the energy of the acceptor ground state is of the order of Bohr energy of a the heavy hole

$$\varepsilon_A = \frac{4}{9}\varepsilon_{hh} = \frac{2m_{hh}^* e^4}{9\chi^2\hbar^2} \tag{8.15}$$

where $m_{hh}$ is the mass of the heavy hole, $\chi$ is the dielectric permeability, $\hbar$ is Planck's constant, then in the magnetic field the acceptor ionization energy is of the order of Bohr energy of the light hole. This dependence of the acceptor ionization energy on the magnetic field strength occurs in magnetic fields, when the light hole becomes quantized. In even stronger fields, when heavy holes become quantized, the ionization energy of the acceptor will again be of the order of heavy hole energy.

The probability of radiative recombination is proportional to the effective volume of the hole wave function. The nonmonotonous dependence of the ionization energy of the acceptor leads to a change in the effective volume of the hole wave function, which according to Galazka et al. should be reflected in the luminescence intensity in the magnetic field [67]. If $B = 0$, the effective volume of the hole wave function is $V_{eff} \sim a_{hh}^3$, where $a_{hh} = \hbar^2\chi/m_{hh}^* e^2$ is the Bohr radius of a heavy hole. It was shown that in semimagnetic semiconductors the hole wave function in a magnetic field is anisotropic [102]. Its transverse size is of the order of $a_\perp = \hbar^2\chi/m_\perp^* e^2$, where $m_\perp = m_0(\tilde{\gamma} + \gamma_1)$, $m_0$ is the free electron mass, $\tilde{\gamma}, \gamma_1$ are the modified Luttinger parameters. The value of $m_\perp^*$ is of the order of light hole mass. The longitudinal size of the wave function is of the order of $a_\perp(m_\perp/m_{hh})^{1/3}$. Thus, $V_{eff}$ increases with increasing the magnetic field strength and reaches values of the order $a_{hh}^{1/3}a_\perp^{8/3}$. In magnetic fields, when the heavy hole becomes quantized, the $V_{eff}$ value will decrease with increasing the magnetic field strength. In the ultra-quantum limit the transverse size of the hole wave function is of the order of the magnetic length $\lambda = (\hbar c/eB)^{1/2}$, and the longitudinal size is $\lambda^{2/3}a_{hh}^{1/3}$, i.e. $\lambda^{8/3}a_{hh}^{1/3}$. Thus, a maximum should be observed on the curve representing the dependence of the photoluminescence intensity upon the magnetic field for the transitions "conduction band-to-acceptor".

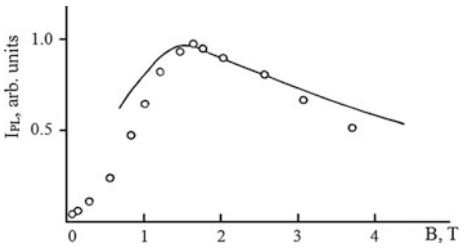


**Fig. 8.15** The dependence of photoluminescence intensity in $Hg_{0.868}Mn_{0.132}Te$ upon the magnetic field, *circles*—experiment, *curve*—theory

The theoretical curve of the dependence of photoluminescence intensity upon the magnetic field strength calculated by Bykhovckiy et al. by using the wave functions of the hole on the acceptor is shown in Fig. 8.15 [102].

The experimental dependence of the photoluminescence intensity upon the magnetic field strength for the transitions "conduction band-to-acceptor" measured at 1.8 K for the $Hg_{0.868}Mn_{0.132}Te$ alloy is shown in the figure for comparison. The presented results demonstrate a good agreement between theory and experiment.

Thus, as a result of the performed research [67, 102], it was conclusively demonstrated that the non-monotonic dependence of the photoluminescence intensity for transitions "conduction band-to-acceptor" upon the magnetic field strength is connected with the behaviour of the ionization energy of the acceptor in a magnetic field. As mentioned above, the magnetic field value at which there is a maximum in the photoluminescence intensity depends on the content of manganese in $Hg_{1-x}Mn_xTe$, $Hg_{1-x-y}Cd_xMn_yTe$.

The experiments confirm also that the increase in the photoluminescence intensity in the magnetic field $B = B_{max}$ decreases with increasing the content of manganese. This behavior of the values $B_{max}$ and $I_{FL}(B = B_{max})$ was explained taking into account the dependence of the ionization energy of the acceptor on the manganese content [65, 67]. It was also shown that the acceptor ionization energy increases with increasing the manganese content in the crystal lattice of the semiconductor [103]. Therefore, the change in the effective volume of the hole wave function at a deep acceptor is less sharp as compared to the change in the effective volume of the wave function of a hole at a shallow acceptor. Since the probability of radiative recombination is proportional to the effective volume of the wave function of the hole on an acceptor, the increase of the photoluminescence intensity in the magnetic field must decrease with increasing the manganese content.

Some oscillations have been observed on the non-monotonic dependence of the photoluminescence intensity as a function of the magnetic field strength for "conduction band-to-acceptor" transitions at high levels of excitation [67]. A certain concentration of nonequilibrium charge carriers is created in the conduction band when the photoluminescence is excited by laser radiation. A definite Fermi level corresponds to the given concentration of non-equilibrium carriers, determined by the excitation level. It was supposed that the oscillation on the dependence $I_{FL} = f(B)$ are connected with the intersection of the Fermi level with the Landau levels in a magnetic field. A method has been developed for the determination of the

concentration of the nonequilibrium carriers and the exchange parameters based on the analysis of the oscillatory structure of photoluminescence spectra in a magnetic field [67]. It was obtained for the integrals of the exchange interaction that $N_0\alpha = -0.45\,\text{eV}, N_0\beta = 0.80\,\text{eV}$. In our opinion, these data obtained directly from the experiment are the most reliable as compared to the large spread of data in the literature for these parameters.

The peculiarities of the photoluminescence spectra of $Hg_{1-x}Mn_xTe$ in a magnetic field for the composition ($0.09 < x < 0.11$) have been discussed by Fuchs et al. [97]. The strong increase of the recombination radiation and the narrowing of the line width to less than 2.5 meV in an external magnetic field was associated with the formation of a magnetic exciton polaron [97].

## 8.6 Magneto-Optical Properties

It is known that in semimagnetic semiconductors the spectrum of charge carriers is greatly modified as a result of the exchange interaction of their spins with the spins of the magnetic impurities. The parameters of the electronic states in such semiconductors are changed when the concentration of magnetic impurities, the temperature or the applied magnetic field is changed. The measurement of the resonant absorption of light in an external magnetic field is a powerful method for studying such states. The magneto-optical properties of $Hg_{1-x}Mn_xTe$ and $Hg_{1-x-y}Cd_xMn_yTe$ semimagnetic alloys were studied in a series of works [104–106]. The combined and cyclotron resonances have been studied in the narrow bandgap $Hg_{1-x-y}Cd_xMn_yTe$ semimagnetic alloys. This study opens up new possibilities for the elucidation of the effect of exchange interaction on the energy spectrum of these materials. The studies of the cyclotron resonance allow to determine The parameters of the energy spectrum are determined from the cyclotron resonance investigations, while the effect of the exchange interaction is assessed from the combined resonance study.

Georgitse et al. measured the optical transmission in a spectral range of 96.52–294.8 μm and a temperature range of 2–12 K in magnetic fields up to $6.5T$ in $n - Hg_{1-x-y}Cd_xMn_yTe(x = 0.03; x = 0.08; y = 0.11; y = 0.12)$ epitaxial solid solutions obtained by liquid-phase epitaxy method in a closed system on substrates of cadmium telluride. The studies were conducted on a laser magnetic spectrometer with $CH_3OH(\lambda = 96.52;\ 118.83;\ 133.2;\ 170.58)$ μm and $CH_3OD(\lambda = 145.66;\ 294.8)$ μm lasers pumped by a tunable $CO_2$ laser in Voigt and Faraday geometry as radiation source. The value of $N_D - N_A$ at 77 K in the investigated samples vary in a range of $(4 \times 10^{14}–1 \times 10^{15})$ $\text{cm}^{-3}$, the compensation degree being $\sim 0.9$. The samples were illuminated during the measurements by radiation from the region of fundamental absorption in order to reduce the influence of nonuniformity in the distribution of impurities. Some lines with a complex structure have been observed in the magneto-absorption spectra [104, 105]. The form of the lines is changed with

changing the temperature. The splitting of the Landau levels in a magnetic field has been calculated using the modified model of Pigeon Brown in order to identify the observed magneto-absorption lines in the spectrum [104, 105]. The following values of the energy spectrum parameters have been used in calculations: $\varepsilon_p = 18.3\,\text{eV}$; $\Delta = 1.0\,\text{eV}$; $\gamma_1 = 3.3$; $\tilde{\gamma} = 0.3$; $k = 0.09$. Assuming that the center of the line corresponds to the cyclotron resonance, it was found that $\varepsilon_g = 0.245\,\text{eV}$ and the effective mass of the electron is $m_e^* = 2.1 \times 10^{-2} m_0$. The following parameters were used for fitting: $N_0\alpha, S_0, T_0$, and the following values were obtained for the best fitting: the efficient spin $S_0 \approx 0.95$; the effective temperature $T_0 = 10.7$ K; and the integral $N_0\alpha = -(0.38 \pm 0.02)$ eV. The energy levels of electrons of the off-diagonal matrix elements of the Hamiltonian have been theoretically calculated taking into account the antiferromagnetic interaction between the manganese ions $Mn^{+2}$. It was shown that this contribution can be neglected for the concentration of manganese ions $Mn^{+2}$(11–12) % in a magnetic field of above $0.8T$. Three conduction band electronic resonances have been identified as a result of spectrum analysis and theoretical calculations [85]: the combined resonance (CR1) $b(1) \rightarrow a(2)$; the cyclotron resonance $a(0) \rightarrow a(1)$; and the combined resonance (CR3) ($a(0) \rightarrow b(1)$). Note that two combined resonances have been observed in the $Hg_{1-x-y}Cd_xMn_yTe$ narrow-gap semimagnetic semiconductor [104, 105]. It was found that the combined resonance CR1 shifts to higher magnetic fields with increasing temperature, while the CR3 shifts to lower magnetic fields. It was observed that the line shape and the position of resonances are identical for the Faraday and the Vogt geometry, which is in contrast with the behaviour of usual semiconductors, wherein the combined resonance can be observed only in the Vogt geometry. It was previously predicted that combined resonances can be observed in semimagnetic semiconductors regardless of the used geometry [107, 108].

The problem of a reliable determination of exchange interaction parameters in semimagnetic semiconductors has still not lost its relevance. The electric dipole spin resonance (EDSR) can be considered as a most direct and therefore a most accurate method of assessing the value of the exchange integral for electrons in the conduction band. The observation of EDSR in the $Hg_{1-x}Mn_xTe$, $Hg_{1-x-y}Cd_xMn_yTe$ systems has been reported by Stepnewski et al. [109] and Georgitse et al. [77]. The observed EDSR line in the system $Hg_{1-x}Mn_xTe$ system proved to be so wide that it was not possible to estimate the value of the exchange integral of conduction band electrons $N_0\alpha$ [109]. At the same time, it was possible to observe quite narrow EDSR lines by a careful selection of $Hg_{1-x-y}Cd_xMn_yTe$ samples [77], and to assess the values of band parameters and the exchange integral $N_0\alpha$ of the conduction band on the basis of the position of magnetic resonances. Georgitse et al. demonstrated the possibility to determine the concentration of free carriers, and the dielectric permittivity from the position of plasma-shifted cyclotron resonance in Vogt geometry in the magnetic field [77].

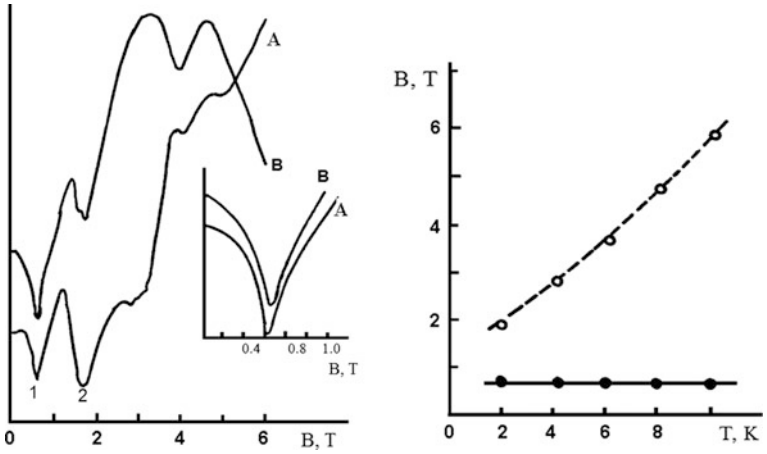


**Fig. 8.16** The spectra of the magneto-transmission for the $Hg_{1-x-y}Cd_xMn_yTe$ alloy in the Farday and Vogt geometries for λ = 294.8 μm at $T$ = 2 K [77]

Figure 8.16 shows the typical spectra of magneto-transmission measured by Georgitse et al. [77] for the $Hg_{0.85}Cd_{0.03}Mn_{0.12}Te$ alloy in Vogt and Faraday geometries for $\lambda = 294.8$ μm at 2 K. The choice of this radiation frequency is conditioned by the fact that it allows to observe various types of spectrally separated resonances, which improves the accuracy of determining the position of resonance lines in a magnetic field. Several resonance lines are observed in this figure, which have been identified by Georgitse et al. [77]. The positions of the line 1 in the Faraday and Voigt geometries are shown in the inset to this figure. One can see that in the Vogt geometry the line are shifted towards lower magnetic fields as compared to the Faraday geometry. This fact was explained as follows [77]: in the Faraday geometry the contribution to the line 1 comes from the cyclotron resonance and from the combined resonance, while in the Vogt geometry it comes from the combined resonance as well as from a resonance with a frequency given by the expression:

$$\omega = \sqrt{\omega_c^2 + \omega_p^2} \tag{8.16}$$

where $\omega_c$ is the cyclotron frequency, $\omega_p^2 = 4\pi Ne^2/m_c^*\chi$ is the electron plasma frequency, $N$ is the concentration of electrons, $m_c^*$ is the electron effective mass, $\chi$ is the dielectric permittivity.

The expression (8.16) is the condition for observing the so-called plasma-shifted cyclotron resonance (PSSR). Georgitse et al. determined the concentration of electrons in the investigated samples by comparing the frequency of CR with that of PSSR making use of the expression (8.16) [77]. For instance, for the $Hg_{0.85}Cd_{0.03}Mn_{0.12}Te$ alloy the plasma frequency is $\omega_p = 3.42 \times 10^{12}\,c^{-1}$, and for

the given $\chi = 16$ the electron density is $N = 1.09 \times 10^{15}\,\mathrm{cm}^{-3}$, which is in agreement with the results of Hall effect measurements. The Fermi level in this case is $\varepsilon_F = 2.1$ meV. Georgitse et al. suggested that the line 2 corresponds to EDSR for the transition $b(0) \rightarrow a(0)$, it being observed in both geometries. The observation of resonances with spin flipping regardless of the selected geometry is possible due to the relaxation of the selection rules in semimagnetic materials [107]. One of the reasons for this relaxation is the giant splitting of the Landau spin sublevels. The energy of the EDSR transition is given by the expression:

$$\Delta\varepsilon = \varepsilon_{a(0)} - \varepsilon_{b(0)} = g_{eff}\mu_B B \tag{8.17}$$

where $\mu_B$ is the Bohr magneton, $B$ is the magnetic field, $g_{eff}$ is the effective g-factor given by the expression:

$$g_{eff} = g^* - \frac{xN_0\alpha\langle S_z\rangle}{\mu_B} \tag{8.18}$$

where $g^*$ is the g-factor of electrons without taking into account the exchange interaction, $\langle S_z\rangle$ is the mean spin.

$$\langle S_z\rangle = -S_0 B_{5/2}(g_{Mn}\mu_B B/k(T + T_0)) \tag{8.19}$$

In this expression, $B_{5/2}$ is the Brillouin function, $g_{Mn}$ is the g-factor of the manganese ions, which value is 2, $k$ is the Boltzmann constant, $T$ is the temperature at which the experiment is conducted.

By using the EDSR position in the magnetic field, the value of $g_{eff}$ has been determined from the expression (8.17), and the value of the exchange integral of the conduction band electrons $N_0\alpha$ has been determined from the expression (8.17). The spin relaxation time $\tau_S = \alpha B/\Delta B\omega_S$ was determined from the half-width of the EDSR line $(\Delta B)$ [77]. It was found that the spin relaxation time in the investigate alloys ranges in the limits of (7–8) $\times\ 10^{-13}$ s and the resonance figure of merit is $\omega_S\tau_S = 4$–5.

The temperature shift of resonances has also been investigated. It was found that the resonances can be classified in two groups according to the temperature dependence. A strong dependence of the line upon temperature is characteristic for the spin resonance. The EDSR line moves to high magnetic fields due to the decrease of magnetization $M = -xN_0 g_{Mn}\mu_B\langle S_z\rangle$ with increasing temperature. A weak temperature dependence is characteristic for the diamagnetic resonance and it is well described by the theory with $d\varepsilon_g/dT = 0.35$ meV/K which is in agreement with the restructuring of the energy spectrum under the influence of temperature.

The values of energy spectrum parameters and of the exchange interaction, calculated from the analysis of magnetic resonances in $Hg_{1-x-y}Cd_xMn_yTe$ semimagnetic alloys are shown in Table 8.1.

The data, obtained for the exchange parameters from the magnetic resonance analysis agree well with the previously obtained results [65–68, 85].

**Table 8.1** The values of energy spectrum parameters and of the exchange interaction in the $Hg_{1-x-y}Cd_xMn_yTe$ semimagnetic alloys

| Samples | $T$, $K$ | $g_{eff}$ | $g^*$ | $N_0\alpha$, $eV$ | $S_0$ | $T_0$ | $m_c^*/m_0$ | $\varepsilon_g$, $V$ $g$ |
|---|---|---|---|---|---|---|---|---|
| $Hg_{0.81}Cd_{0.08}$ $Mn_{0.11}Te$ | 2 | 19.1 | −37.6 | −(0.35 ± 0.02) | 0.95 | 10.7 | $2.1 \times 10^{-2}$ | 0.245 |
| | 4.2 | 14.7 | | | | | | |
| $Hg_{0.85}Cd_{0.03}$ $Mn_{0.12}Te$ | 2 | 40.4 | −44.2 | −(0.41 ± 0.02) | 0.87 | 11.6 | $1.85 \times 10^{-2}$ | 0.215 |
| | 4.2 | 25.1 | | | 0.89 | 11.2 | | |
| | 6 | 19 | | | 0.9 | 10.7 | | |
| | 8 | 15.1 | | | 0.92 | 10.3 | | |
| | 10 | 12.2 | | | 0.93 | 9.7 | | |

## 8.7 ODMR in Semimagnetic Semiconductors. Optical Orientation

ODMR is based on the phenomenon of resonance effects of microwave fields on the optical characteristics of a system. Such effects may be due to both the individual properties of charge carriers, and the spin-dependent phenomena related to the interaction of carriers with external electric and magnetic fields. The first information about the research of ODMR in semimagnetic structures was reported by Georgitse et al. [85], with a $Hg_{1-x}Mn_xTe$ solid solution with a high manganese content $x > 0.2$ and p-type conductivity with impurity concentration of $\sim 10^{15}$ cm$^{-3}$ as the object of the research. Two resonances were observed in the ODMR spectra measured at 2 K. The first resonance observed in a field of $0.2T$ was assumed to be due to the electron spin resonance (ESR) of holes bound to an acceptor ($g = 12 \pm 1$), while the second resonance, the so-called magnetic dipole resonance, observed in a field of $1.15T$ is due to the magnetic dipole interaction between the manganese ions $Mn^{+2}$ ($g \approx 2.0$). The analysis of experimental results enabled to determine the spin relaxation time, as well as the internal magnetic field in $Hg_{1-x}Mn_xTe$ ($x > 0.2$) alloys [85].

The spin orientation of electrons has been inevestigated at a temperature of 4.2 K under excitation by circularly polarized light with the energy close to the bandgap of non-magnetic alloys $Hg_{0.69}Cd_{0.31}Te$ and $Hg_{0.39}Cd_{0.61}Te$, as well as close to the parameters of the energy spectrum of the $Hg_{0.77}Mn_{0.23}Te$ semimagnetic alloy [110]. The mechanisms of spin relaxation of electrons in $Hg_{1-x}Cd_xTe$ and $Hg_{1-x}Mn_xTe$ have been analysed. A careful analysis of the experimental results proved that the Beer-Aronov Picus spin relaxation mechanism plays a significant role in $Hg_{1-x}Cd_xTe$ alloys at low temperatures, while in $Hg_{1-x}Mn_xTe$ semimagnetic alloys the spin relaxation is due to the exchange interaction of nonequilibrium electrons with the manganese ions [110]. The spin relaxation time was determined in $Hg_{1-x}Mn_xTe$ alloys, and the concentration of deep recombination centres was estimated.

## 8.8 Photoreceivers Based on $Hg_{1-x}Mn_xTe$, $Hg_{1-x-y}Cd_xMn_yTe$

The first reports about the photovoltaic receivers based on $Hg_{1-x}Mn_xTe$ and $Hg_{1-x-y}Cd_xMn_yTe$ solid solutions have been published in 1986 [111, 112]. The carrier transporter mechanisms in photodiodes have been investigated in the next years, and the parameters of devices have been improved [113, 114]. It was demonstrated that the current flow in the temperature range from liquid nitrogen to 250 K is determined by the thermal activation mechanisms [115], it being governed by a diffusion mechanism at $T > 110$ K, and by a generation-recombination mechanism at T < 110 K. The reverse currents at a bias of 1 V do not exceed 1 nA, and the value of $R_oA$ at 85 K was found to be of $1.7 \times 10^7$ Ω·cm$^2$. These values, in our opinion, are record ones for $Hg_{1-x}Mn_xTe$, $Hg_{1-x-y}Cd_xMn_yTe$ diodes of similar composition. The specific detectivity at 77 K and at a backlight aperture of $2\pi sr$ was found to be $\sim 5 \times 10^{11}$ Hz$^{1/2}$Вт$^{-1}$, which corresponds to the BLIP regime. These parameters are at a level corresponding to the best diodes on $Hg_{1-x}Cd_xTe$, and the photodiodes are sensitive for $\lambda_{1/2} = 3.8$ μm at the temperature of 77 K [115]. The obtained results demonstrate that the technology for producing epitaxial layers $Hg_{1-x-y}Cd_xMn_yTe$ layers is at the same level as the previously developed technology for $Hg_{1-x}Cd_xTe$ laters. On the other hand, one can expect that the photodiodes on $Hg_{1-x-y}Cd_xMn_yTe$ solid solutions will demonstrate better stability due to the higher structural perfection of these solid solutions. Note that only a few publications are available on photodetectors based on $Hg_{1-x}Mn_xTe$ and $Hg_{1-x-y}Cd_xMn_yTe$, (a review of early work is given by Pawlikowski [11]), whereas there are many studies on $Hg_{1-x}Cd_xTe$ with various types of photodetectors (photoconductive, photovoltaic, SPRITE-type, etc.), (see, e.g. [116–121]).

## 8.9 Conclusions

The semimagnetic $Hg_{1-x}Mn_xTe$ semiconductors are attractive primarily due to higher mechanical strength and thermal stability as computed to $Hg_{1-x}Cd_xTe$. The possibility of obtaining materials with the same bandgap parameters but with different contents of manganese in the quaternary $Hg_{1-x-y}Cd_xMn_yTe$ alloys system by changing the relative content of cadmium and manganese, apart from a purely scientific interest, has also a special practical interest. Therefore, the semimagnetic semiconductors $Hg_{1-x}Mn_xTe$, $Hg_{1-x-y}Cd_xMn_yTe$ have a series of advantages as materials for the creation of infrared detectors and infrared lasers as compared to their non-magnetic $Hg_{1-x}Cd_xTe$ counterparts.

## References


1. R.T. Delvis, B. Lewis, J. Phys Solids **24**, 549 (1968)
2. P. Becla, P.A. Wolff, R.L. Aggarwal, S.Y. Tuen, R.R. Galazka, J. Vac. Sci. Technol. A **3**(1), 119 (1985)
3. N.L. Bazhenov, V.I. Ivanov- Omskii, K.E. Mironov, V.R. Movila, FTP **22**, 1258 (1988)
4. N.L. Bazhenov, S.I. Gasanov, V.I. Ivanov-Omskii, V.R. Movila, Lett. JETF **17**, 48 (1990)
5. J.K. Furdyna, Appl. Phys. **64**, R29 (1988)
6. B.A. Bunker, W.F. Pong, V. Debska, D.R. Yorder-Shortand, J.K. Furdyna, in *Diluted Magnetic (Semimagnetic) Semiconductors*, vol. 89, ed. by R.L. Aggarwal, J.K. Furdyna, S. Molnar (Materials Research Society, Pittsburg, 1987), p. 231
7. W. Girrat, J.K. Furdyna, in *Semiconductors and Semimetals*, vol. 25, ed. by R.K. Willardson, A.C. Becr, J.K. Furdyna, I. Kossut (Academic, Boston, 1988), p. 1
8. J.K.J. Furdyna, Vac. Sci Technol. **21**, 220 (1982)
9. A. Rogalski, Infrared Phys. **31**, 117 (1991)
10. I.I. Lyapilin, I.M. Tsidilkovskii, UFN **146**, 35 (1985)
11. I.M. Pawlikowski, Infrared Phys. **3**, 295 (1990)
12. A. Wall, C. Caprile, A. Franciosi, R. Reifenberger, U. Debska, J. Vac. Sci. Technol. **A4**, 818 (1986)
13. I. Piotrowski, W. Galus, M. Grudrien, Infrared Phys. **31**, 1 (1991)
14. W.M. Higgins, G.N. Pultz, R.G. Roy, R.A. Lancaster, I.L. Schmit, J. Vac. Sci. Technol. **A7**, 271 (1989)
15. A. Schenk, Phys. Stat. Solidi (a) **122**, 413 (1991)
16. E.O. Kane, J. Phys. Chem. Solids **1**, 249 (1957)
17. S. Datta, J.K. Furdyna R.L. Gunshor, Superlattices Microstruct. **1**, 327 (1985)
18. R.L. Gunshor, M. Otsuka, M. Yamanishi, L.A. Kolodzeijski, T.C. Bonsett, R.B. Bylsma, S. Datta, J.K. Furdyna, J. Cryst. Growth **72**, 294 (1985)
19. R.B. Galzka, I. Kossut, *Lecture Notes in Physics,* vol 132 (Springer, Berlin, 1980), p. 245
20. I. Mycielski, in *Recent Developments Metter Physics*, ed. by I.T. Devreese (Plenum, New York, 1981), p. 257
21. I. Kossut, in *Semiconductors and Semimetals*, vol. 25, ed. by R.K. Willardson, A.C. Beer, J. K. Furdyna, I. Kossut (Academic, Boston, 1988), p. 183
22. I. Mycielski, in *Semiconductors and Semimetals*, vol. 25, ed. by R.K. Willardson, A.C. Beer, I. K. Furdyna, I. Kossut (Academic, Boston, 1988), p. 311
23. G. Bastard, C. Rigaux, Y. Guldner, A. Mycielski, J.K. Furdyna, D. Mullin, Phys. Rev. **24**, 1961 (1981)
24. C.R. Pidgenon, R.N. Brown, Phys. Rew. **146**, 575 (1966)
25. M. Jaczinski, I. Kossut, R. Galazka, Phys. Stat. Solidi (b) **88**, 73 (1978)
26. A. Rogalski, K. Iozwikowski, Phys. Stat. Solidi (a) **122**, K39 (1991)
27. N.P. Gavaleshko, P.N. Gorley, V.A. Shenderovsky, Narrow-Gap Semiconductors. Preparation and Physical Properties. (Kiev, 288, 1984)
28. R.B. Galazka, I. Kossut, L. Bornstein, *New Series 17b* (Springer, Berlin, 1982), p. 302
29. I. Kaniewski, A. Mycielski, Solid Stat. Commun. **41**, 959 (1982)
30. A. Jozwikowska, K. Jozwikowski, A. Rogalski, Infrared Phys. **31**, 543 (1991)
31. I.D. Wiley, R.N. Dexter, Phys. Rev. **181**, 1181 (1969)
32. U. Debesk, T. Dietl, G. Grabeski, E. Ianck, Phys. Stat. Solidi (a) **64**, 707 (1981)
33. N.L. Bazhenov, S.I. Hasanov, V.I. Ivanov-Omskii, K.E. Mironov, K.D. Mynbayev, FTP **25**, 2345 (1991)
34. N.L. Bazhenov, S.I. Hasanov, Ivanov- Omskii V.I. Tech. Phys. Lett. **17**, 9 (1991)
35. L.A. Kosyachenko, A.V. Markov, S.E. Ostapov, I.M. Rarenko, V.M. Sklyarchuk, E.F. Sklyarchuk, FTP **36**, 1217 (2002)
36. N.P. Gavaleshko, V.V. Teterin, F.F. Sizov, S.J. Paranchich, FTP **27**, 459 (1943)

37. E.I. Gheorghita, A.E. Gheorghita, P.G. Untila, in *Materials of the IVth Conference on Physics of Crystalline and Amorphous States in Semiconductors* (Iasi, 1996)
38. N.L. Bazhenov, V.I. Ivanov-Omskii, K.E. Mironov, V.F. Movila, FTP **22**, 1258 (1988)
39. N.B. Brandt, V.V. Moshchalkov, L.O. Orlov, JETF **84**, 1059 (1983)
40. I. Newodniczanska-Zawadzka, R. Protrowski, J. Kossut, J. Cryst Growth **72**, 384 (1985)
41. E.I. Gheorghita, V.I. Ivanov-Omskii, K.E. Mironov, P.G. Untila, Proceedings of the universities of the USSR. Physics **3**, 96 (1990)
42. E.I. Gheorghita, V.I. Ivanov-Omskii, K.E. Mironov, P.G. Untila, Proceedings of the universities of the USSR. Physics **4**, 114 (1990)
43. L.P. Zverev, V.V. Kruzhayev, G.M. Minkov, O.E. Rut, N.P. Gavaleshko, V.M. Frasunyak, JETF **86**, 1073 (1984)
44. R.G. Mani, T. McNair, C.R. Lu, R. Crober, J. Cryst. Growth **97**, 617 (1989)
45. P.I. Baranskiy, A.Ye. Belyayev, O.A. Bodnaruk, I.N. Gorbatyuk, S.M. Komirenko, I.M. Rarenko, N.V. Shevchenko, FTP **24**, 1490 (1990)
46. T. Piotrowski, J.W. Tomm, N. Puhlmann, Phys. Stat. Solidi (a) **117**, K181 (1990)
47. N.G. Garbuz, S.V. Kondrakov, S.A. Popov, E.V. Susov, A.V. Filatov, R.A. Khaziyeva, E.N. Holina, Izv. AN SSSR. Inorg. Mater. **26**, 536 (1990)
48. R.E. Kremer, J. Tang, F.G. Moore, J. Cryst. Growth **86**, 797 (1988)
49. Chen Chenjia, Liu Jirhou, Zhang Bei, Rong Zuxii, Rare Met. **9**, 272 (1990)
50. P. Brogowski, T. Piotrowski, Semicond. Sci Technol. **6**, 530 (1990)
51. V.D. Prozorovskiy, IYu. Zreshidova, SYu. Paranchich, L.D. Paranchich, FTT **31**, 326 (1989)
52. A.E. Belyayev, YuG Semenov, N.V. Shevchenko, Tech. Phys. Lett. **51**, 164 (1990)
53. A.E. Belyayev, YuG Semenov, N.V. Shevchenko, Tech. Phys. Lett. **53**, 519 (1991)
54. R.I. Bashirov, V.A. Yelizarov, N.Yu. Matveyeva, FTP **28**, 519 (1994)
55. F. Capper, J. Vac. Sci. Technol. B **9**, 1666 (1961)
56. A.V. Gorshkov, Highly-pure materials. **207**, (1989)
57. M.I. Ibragimova, N.S. Baryshev, I.B. Khaybullin, F.I. Akhmedova, A.P. Fadeyeva, FTP **23**, 1249 (1989)
58. K.E. Mironov, P.G. Untila, O.V. Zelenova, in *Proceedings of the VIIth All-Union Symposium `Semiconductors with a Narrow Band Gap and Semimaterials*, vol. 148 (Lvov, 1986)
59. M.M. Trifonova, N.S. Baryshev, M.P. Mezentseva, FTP **25**, 1014 (1991)
60. M.M. Trifonova, N.S. Baryshev, M.P. Mezentseva, FTP **26**, (1992)
61. M.M. Trifonova, N.S. Baryshev, I.S. Averyanov, in *Proceedings of Rep. III All-Union. Sci-tech. Conference Materials of Chalcogenide Semiconductors,* vol. 1 (Chernovtsy, 1991), p. 69
62. N.S. Baryshev, M.M. Trifonova, M.P. Mezentseva, I.S. Averyanov, in *Proceedings of Report XXIX of the Conference. In low-temperature physics, Tez. dokl. XXIX Conference in Low-Temperature Physics*, vol. 342 (Kazan, 1992)
63. M. Ortenberg, Semicond. Sci. Technol. **8**, 566 (1993)
64. V.I. Ivanov-Omskii, N.N. Berchenko, A.I. Elizarov, Phys. Stat. Solidi (a) **163**, 11 (1987)
65. B.L. Gelmont, R.R. Golonska, V.I. Ivanov-Omskii, I.T. Postolaki, V.A. Smirnov, FTP **20**, 73 (1986)
66. Ye.I. Georgitse, V.I. Ivanov-Omskii, V.M. Pogorletski, T. Piotrovskiy, V.A. Smirnov, FTP **24**, 1732 (1990)
67. R.R. Galazka, B.L. Gelmont, V.I. Ivanov-Omskii, I.T. Postolaki, V.A. Smirnov, Solid Stat. Commun. **58**, 311 (1986)
68. Ye.I. Georgitse, V.I. Ivanov-Omskii, V.R. Masterov, V.M. Pogorletski, V.A. Smirnov, FTP **24**, 2160 (1990)
69. L. Dobacrewski, E. Jenik, G. Karcrewski, Acta Phys. Pol. A **75**, 63 (1989)
70. V.Ye. Begovatov, N.S. Baryshev, N.N. Belyy, M.N. Bryazkiy, I.N. Gorbatyuk, FTP **23**, 2074 (1989)
71. P.I. Baranskiy, A.E. Belyayev, I.N. Gorbatyuk, S.M. Komirenko, N.M. Rarenko, N.V. Shevchenko, FTP **25**, 1183 (1991)

72. E.I. Georgitse, I.T. Postolaki, V.M. Pogorletski, P.G. Untila, V.A. Smirnov, V.A. Maltseva, Izv. AN MSSR. Phys. Mech. **14** (1990)
73. T.I. Nazarenkova, E.I. Salkov, N.V. Sochinskiy, FTP **23**, 1309 (1989)
74. N.V. Sochinskiy, T.I. Nazarenkova, I.S. Bakim, B.I. Khizhnyak, in *Materials of All-Union Seminar of Impurities and Defects in Narrow-Gap Semiconductors*, vol. 72 (Pavlodar, 1989)
75. N.S. Baryshev, V.E. Begovatov, M.P. Mezentseva, Trifanova, Averyanov I.S. Inorg. Mater. **27**, 2536 (1991)
76. N.S. Baryshev, V.E. Begovatov, I.S. Averyanov, Thez. in *Report of the II-nd scientific. Conference. The Photoelectric Phenomena in Semiconductors* (Ashkhabad, 1991), p. 72
77. E.I. Georgitse, V.I. Ivanov-Omskii, V.F. Movila, D.I. Tsypishka, FTP **25**, 41 (1991)
78. K. Takita, T. Uchinc, T. Ipposhe, K. Masuda, Solid. Stat Commun. **56**, 603 (1985)
79. T. Uchinc, K. Takita, K. Masuda, J. Phys. Soc. Jpn. **58**, 627 (1989)
80. K. Takita, T. Uchnco, K. Masuda, Semicond. Sci. Technol. **5**, 5277 (1990)
81. N.S. Baryshev, in *Materials of All-Union Seminar of Impurities and Defects in Narrow-Gap Semiconductors* (Pavlodar, 1989), p. 135
82. N.S. Baryshev, B.L. Gelmont, M.I. Ibragimova, FTP **24**, 209 (1990)
83. O.A. Bonaruk, A.A. Vertiy, I.N. Gorbatyuk, I.V. Ivanchenko, N.A. Popenko, I.M. Rarenko, S.I. Tiratov, FTP **30**, 1236 (1996)
84. S.G. Gasan-Zade, V.I. Kalenik, G.A. Shepelskiy, FTP **30**, 63 (1996)
85. E.I. Georgitse, V.V. Dyakonov, V.I. Ivanov-Omskii, V.M. Pogorletski, N.G. Romanov, V.A. Smirnov, Tech. Phys. Lett. **16**, 74 (1990)
86. I. Postolaki, University education from Moldova to 75 years, in *The Conference Scientific-Methodological Materials*, vol. III (Chisinau, 2005), p. 85
87. V. Kantser, E. Georgitse, L. Gutsuleak, I. Postolaki, in *VIIth Russian Conference on Semiconductor Physics* (Moscow, 2005), p. 145
88. I. Postolaki, New resercarch trends in materials science. ARM-4 Proc. **I**, 383, (2005). Constanta
89. I.T. Postolaki, in *VIIth Russian Conference on Semiconductor Physics* (Moscow, 2005), p. 143
90. I. Postolaki, in *Conference of Physicists from Moldova* (*CFM-2005*) (Chisinau, 2005), p. 53
91. Yu.I. Mazur, Semicond. Phys. Quant. Electron. Optoelectron. **1**, 33 (1999)
92. Yu.I. Mazur, S.I. Kriven, G.G. Tarasov, N.V. Shevchenko, Semicond. Sci. Technol. **8**, 1187 (1993)
93. G.G. Tarasov, YuI Mazur, J.W. Tomm, V. Jahnke, Phys. Rev. B **52**, R11565 (1995)
94. Yu.I. Mazur, G.G. Tarasov, V. Jahnke, J.W. Tomm, W. Hoerstel, Semicond. Sci. Technol. **11**, 1291 (1996)
95. G.G. Tarasov, Yu.I. Mazur, S.R. Lavoric, J.W. Tomm, J. Cryst. Growth, **184**(185), 1214 (1998)
96. S.E. Ostapov, I.M. Rarenko, M.D. Timochenko, Semicond. Phys. Quant. Electron. Optoelectron. **7**, 339 (2004)
97. Yu.I. Mazur, Semicond. Phys. Quant. Electron. Optoelectron. **1**, 33 (1998)
98. G.G. Tarasov, Yu.I. Mazur, M.P. Lisitsat et al., Semicond. Sci. Technol. **14**, 187 (1999)
99. V.F. Radantsev, A.M. Yafyasov, V.B. Bogevolnov, Semicond. Sci. Technol. **16**, 320 (2001)
100. F. Fuchs, K. Kheng, K. Schwarz, P. Koidl, Semicond. Sci. Technol. **8**, S75 (1993)
101. A. Mycielski, J. Mysielski, J. Phys. Soc. Jpn. **49**, 807 (1980)
102. A.D. Bykhovckiy, E.M. Vakhabova, B.L. Gelmont, A.A. Efros, FTP **18**, 2094 (1984)
103. T. Woitowica, A. Mysielski, Acta Phys. Pol. **67**, 363 (1985)
104. E.I. Georgitse, V.I. Ivanov-Omskii, V.F. Movila, D.I. Tsypishka, FTP **24**, 1823 (1990)
105. E.I. Georgitse, V.I. Ivanov-Omskii, V.F. Movila, D.I. Tsypishka, in *Proceedings of the VIIIth All-Union Symposium Semiconductors with a Narrow Band Gap, and Semimetals*. Lvov **124** (1991)
106. M. Dobrovolska, Semicond. Sci. Technol. 5159 (1990)
107. Yu.G. Rubo, L.S. Khazan, V.I. Sheka, A.S. Ioselevich, Tech. Phys. Lett. **48**, 30 (1988)
108. Yu.G. Rubo, L.S. Khazan, V.I. Sheka, E.V. Mozdor, Tech. Phys. Lett. **95**, 1880 (1989)

109. R. Stepnewski, M. Grinberg, Acta Phys. Pol. A **67**, 373 (1985)
110. E.I. Georgitse, V.I. Ivanov-Omskii, V.M. Pogorletskii, V.A. Smirnov, Semicond. Sci. Technol. **6**, 924 (1991)
111. P. Becla, J. Vac. Sci Technol. **A4**, 2014 (1986)
112. S. Wong, P. Becla, J. Vac. Sci. Technol. **A4**, 2019 (1986)
113. E. Janik, G. Karczewski, Acta Phys. Pol. **A 73**, 439 (1988)
114. E. Placzek-Popko, L. Jedral, Infrared Phys **26**, 249 (1988)
115. N.L. Bazhenov, S.I. Gasanov, V.I. Ivanov-Omskii, K.E. Mironov, V.F. Movila, Tech. Phys. Lett. **17**, 48 (1991)
116. N.R. Aigina, P.A. Bogomolov, V.I. Sidorov, Foreign electronic appliances. **3** (1982)
117. N.R. Aigina, P.A. Bogomolov, V.I. Sidorov, Foreign electronic appliances. **3** (1984)
118. C.T. Elliot, J. Cryst. Growth **72**, 453 (1985)
119. A. Rogalski, J. Piotrowski, Progr. Quant. Electron. **12**, 87 (1988)
120. N.L. Bazhenov, S.I. Gasanov, V.K. Ogorodnikov, V.I. Protsyk, Foreign electronic appliances. **3** (1986)
121. A.V. Voytsekhovskiy, I.I. Ijnin, V.A. Kemarskiy, N.A. Kulchitskiy, Foreign electronic appliances. **3** (1991)